# Investigation of Strength of Glass Plates with Hole Subjected to Out-of-plane Bending

by

Jan Cervenka

A Report Submitted to the Faculty of the

Milwaukee School of Engineering

in Partial Fulfillment of the

Requirements for the Degree of

Master of Science in Structural Engineering

Milwaukee, Wisconsin

May 2016

**Abstract**

Structural glass facades, distinguished architectural features, are widely used in modern building construction. Understanding the strength of such point-supported glass plates is crucial in the design process. As an analogy to this problem, this research investigates the strength of glass plates subjected to out-of-plane bending and the effects of stress concentration around a hole. The strength of fully tempered ½ inch monolithic and fully tempered ¼ inch – PVB interlayer – ¼ inch laminated glass specimens was determined using a destructive method. Four different monolithic glass specimen types were utilized: those without a hole subjected to four-point bending, those with a hole subjected to four-point bending, those with a hole loaded via a standard swivel fitting (three-point bending), and those with a hole with a chamfered edge subjected to four-point bending. This led to a deeper understanding of the behavior of glass plates near the fitting, and determined the influence of stress concentration on the overall strength of a glass plate. Ultimate stresses were obtained based on the stress concentration factor determined from the Finite Element Model (FEM), thick plate and thin plate analytical models, and readings from strain gauges applied to some of the specimens. The discoveries of this research demonstrate that the drilling method introduces a 3% reduction in the strength of a monolithic glass plate. If the load is applied through the fitting, the strength of a monolithic glass plate is reduced by an additional 13%. The breakthrough discovery made during this process is that chamfering the edge of a hole varies the peak breaking stresses, which results in 18% greater moment capacity.

**Acknowledgments**

My greatest thanks belong to the staff of Stutzki Engineering Inc., namely Mr. Christian Stutzki and Mr. John Knowles, who have greatly contributed to my research project by providing me with their expert and professional knowledge. Not only have they given me guidance on glass industry standards and important background information related to glass behavior, but they have also supplied me with the software and code standards required for this research project to be a success.

I would also like to thank Dr. Douglas Stahl for his patience and continued support throughout this research project as my faculty advisor. His insight and knowledge were key in assisting me throughout the entire process. I would also like to recognize Dr. Stahl for introducing me to the glass industry, which has given my life a new direction professionally. Thank you. In addition, I owe many thanks to my supervising committee members, Dr. Huttelmaier and Dr. Schultz, for their adept advice and expertise.

Additionally, I would like to show my gratitude to Ms. Alyssa Shaff who had the patience and dedication to proofread and linguistically correct every section of this research project as English is not my first language. She has also been a great support and counter opinion during my studies.

Lastly, but certainly not least of all, I am grateful to my family for helping me accomplish my goals. Without their support, I would not have been able to attend this program and finish my studies. I am very grateful for all of their encouragement and assistance, and as acknowledgement I dedicate this research project to them.

**Table of Contents**

**List of Figures**

**List of Tables**

**Nomenclature**

*Symbols*

$a$ = Smallest in-plane dimension of bending of laminate plate

$a_c$ = Critical crack length

$b$ = Glass specimen width

$d$ = Hole diameter

$d_b$ = Loading and bearing edge diameter

$d_{BOTTOM}$ = Bottom ply glass specimen hole diameter

$d_h$ = Glass specimen hole diameter

$d_{TOP}$ = Top ply glass specimen hole diameter

$E$ = Young's modulus of elasticity

$G$ = Shear modulus

$H$ = Plate width

$h$ = Plate thickness

$h_1$ = Thickness of top glass laminate

$h_2$ = Thickness of bottom glass laminate

$h_{ef;w}$ = Effective thickness of laminated glass used for deflection calculations

$h_{ef;\sigma}$ = Effective thickness of laminated glass used for stress calculations

$h_v$ = Thickness of PVB interlayer

$I$ = Moment of inertia

$K$ = Stress intensity factor

$K_{gross}$ = Gross section stress concentration factor

$K_n$ = Bessel's functions of n-th order

$K_{net}$ = Net section stress concentration factor

$K_{netEXP}$ = Net section stress concentration factor determined experimentally from strain gauges

$K_{net\text{-}chamfer}$ = Net section stress concentration factor for chamfered edge of hole

$K_{netROARK}$ = Net section stress concentration factor determined using Roark's formula

$L$ = Glass specimen length

$L_b$ = Loading and bearing edge length

$M_0$ = Uniaxial bending moment

$M_{max}$ = Maximum uniaxial bending moment

$M_t$ = Bending moment in the radial coordinates

$M_y$ = Bending moment about the y-axis

$M_{y(max)}$ = Maximum bending moment about the y-axis

$r$ = Hole radius

$r_0$ = Atom spacing

$S$ = In-plane stresses

$s_b$ = Bearing edge spacing

$S_{gross}$ = Gross section modulus

$s_l$ = Loading edge spacing

$S_{net}$ = Net section modulus

$t$ = Glass specimen thickness

$t_{avg}$ = Average thickness of monolithic glass specimens in one specimen type group

$t_{BOTTOM}$ = Bottom glass ply thickness

$t_{eff}$ = Effective glass thickness calculated per ASTM E1300

$t_{eff\text{-}avg}$ = Average thickness of laminated glass specimens in one specimen type group

$T_g$ = Transition temperature at which glass becomes soft material

$t_{INTERLAYER}$ = PVB interlayer thickness

$t_p$ = Plate thickness

$t_{TOP}$ = Top glass ply thickness

$V(x)$ = Shear stress

$Y$ = Correction factor

$\alpha_1$ = Coefficient of thermal expansion below transient temperature

$\alpha_2$ = Coefficient of thermal expansion above transient temperature

$\gamma$ = Fracture surface energy

$\epsilon_{net}$ = Average net section strain

$\epsilon_{peak}$ = Maximum strain at cross-section

$\theta$ = Angle that defines the radial coordinates

$\mu$ = Friction coefficient

$\nu$ = Poisson's ratio

$\rho$ = Density

$\sigma_{allowable}$ = Allowable edge stress per ASTM E1300

$\sigma_{chamfer\text{-}avg}$ = Average net section stress for specimens with chamfered edge of a hole

$\sigma_{chamfer\text{-}ult}$ = Ultimate strength of monolithic fully tempered glass specimens with chamfered edge of a hole

$\sigma_f$ = Failure stress

$\sigma_{fitting\text{-}lam}$ = Ultimate strength of laminated fully tempered glass specimens loaded via standard swivel fitting

$\sigma_{fitting\text{-}ult}$ = Ultimate strength of monolithic fully tempered glass specimens loaded via standard swivel fitting

$\sigma_{gross}$ = Average gross section stress

$\sigma_{hole\text{-}ult}$ = Ultimate strength of monolithic fully tempered glass specimens with hole

$\sigma_{hole\text{-}lam}$ = Ultimate strength of laminated fully tempered glass specimens with hole

$\sigma_{m}$ = Orowan stress

$\sigma_{n}$ = Nominal tensile stress exposed on glass cracks

$\sigma_{net}$ = Average net section stress

$\sigma_{peak}$ = Maximum stress at the crossection

$\sigma_{peakABAQUS}$ = Peak stress determined using finite element program

$\sigma_{peakREISSNER}$ = Peak stress determined using Reissner's thick plate theory

$\sigma_{peakROARK}$ = Peak stress determined using Roark's formula

$\sigma_{ult}$ = Ultimate strength of monolithic fully tempered glass

$\sigma_{ult\text{-}lam}$ = Ultimate strength of laminated fully tempered glass

*Abbreviations*

| | |
|---|---|
| AAMA | American Architectural Manufacturers Association |
| ASTM | American Society for Testing and Materials |
| COV | Coefficient of variation |
| CTE | Coefficient of thermal expansion |
| EVA | Ethylene vinyl acetate |

| | |
|---|---|
| FEA | Finite element analysis |
| FEM | Finite element model |
| Lbf | pound-force |
| LVDT | Linear variable displacement transducer |
| PVB | Polyvinyl butyral |
| SG | Strain gauge |

# 1. INTRODUCTION

## 1.1. Background Information

"You need to feel the space." These are the famous words of the renowned architect, Mies van der Rohe. His life philosophy was to design structures that are defined by simple construction elements, clear in shape, dignified in expression, perfect in dimension, and harmonious in their details [1]. He designed very subtle and light buildings that emphasized their big space free of heavy bearing systems. His masterpieces include The Crown Hall (Chicago, USA – see Figure 1), Neue Natinalgalerie (Berlin, Germany), and the Tugendhat house (Brno, Czech Republic). He utilized structural glass extensively to open up space and allow occupants to experience the feeling of flowing space. For all of his designs, he was able to connect the outside environment with the inside of a building to achieve this free flow of space.

**Figure 1: The Crown Hall [2].**

Mies van der Rohe was not the only architect to use structural glass to modernize the appearance of buildings and to create an open space feel for its occupants. There are many examples of beautifully designed glass structures that express the unique character of each architect. The Louvre Pyramid (Paris, France – see Figure 2) was designed by I. M. Pei and is distinguished because of its clean and structurally balanced glass construction [3]. The Gherkin (London, UK), designed by Norman Foster, has a very modern and energetic exterior [4]. The Crystal Cathedral (Garden Grove, CA, USA – see Figure 3) is a unique expression of pure structural glass architecture designed by Philip Johnson [5]. There are countless buildings beyond these well-known structures that demonstrate how structural glass can be utilized.

**Figure 2: The Louvre [6].**

## 1.2. Point-Supported Glass

Glass presents great architectural opportunities when used in modern structural assemblies, which is why structural glass has become so popular among various architects over the last sixty years [7]. With this increase in demand for structural glass, many new types of structural support for glass elements have evolved. One key development has been "point

**Figure 3: The Crystal Cathedral [5].**

support" for glass, which means discrete structural connectors are used to support the glass pane rather than the traditional continuous edge support [8].

One such structural engineering firm that focuses specifically on glass is Stutzki Engineering, Inc. [9]. This company produces custom structural assemblies for the unusual glass structures of the commercial and residential industry. The following figures display Stutzki Engineering's expertise. Figure 4 shows a glass fin façade of a newly constructed hospital. Each outside glass pane is supported by interior glass fins using custom made steel fittings. The interior fin façade is supported by very slender columns to highlight the architect's intention of upward direction. Another work seen in Figure 5 shows an architectural chandelier of point-supported glass panes at the Fashion Mall at Keystone in Indianapolis. A set of translucent laminated glass panes are point-supported underneath the skylight to form the circular shape of the chandelier. As another example, Figure 6 depicts a main driveway entrance canopy at Dartmouth Hitchcock Medical Center. These laminated glass panes are also point-supported and provide shelter against rain.

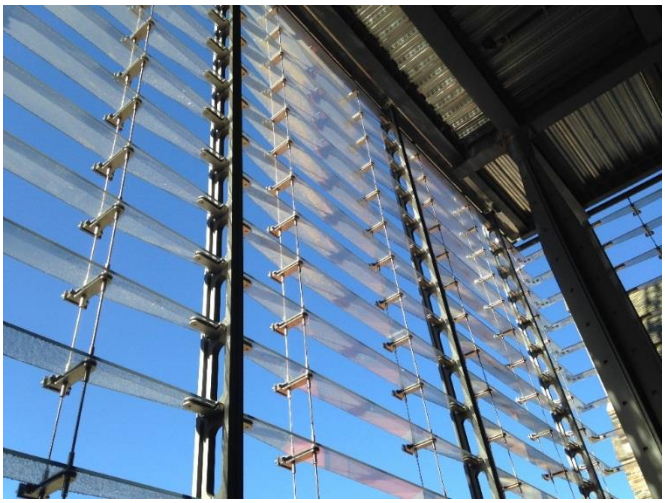

**Figure 4: Glass Fin Facade [10].**

**Figure 5: Glass Chandelier [10].**

To achieve this point support technique, glass structural panes are clamped into a stainless steel swivel fitting that connects the pane to other parts of the structure. A glass pane is usually supported in each of its four corners to provide a symmetrical look as well as to attain even load distribution. For example, Figure 7 shows a standard swivel fitting that clamps the glass in the water-jet drilled hole. The swivel fitting depicted in Figure 7 is mounted to a spider fitting that is directly mounted to a structure.

**Figure 6: Glass Canopy [10].**

Additionally, Figure 8 shows a detail of a typical corner connection of glass panes in a glass façade.

**Figure 7: Swivel Fitting [11].**

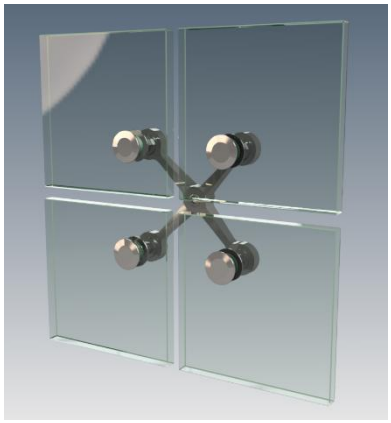

**Figure 8: Point-Support Assembly [10].**

Four-point-supported glass is usually subjected to negative out-of-plane pressure in the form of wind load if it is part of a façade; it is subjected to positive out-of-plane pressure in the form of snow load if it is a member of the canopy structure. This pressure load is applied to the entire glass pane surface creating a positive moment region in the central area and negative moment regions over the supports. The key load effect investigated in this project is the bending moment in the diagonal direction of the four-point-supported glass pane in the region of the point support. This diagonal cross-section can be modeled as a beam-like rectangular glass strip subjected to pressure distributed along its length and is point-supported near its ends. Figure 9 graphically explains this idea of glass pane beam behavior. The local peak of bending moment in the pane coincides with the hole for the point-support fitting. Also, a stress concentration factor associated with the hole creates higher stresses than would be found by simply dividing the moment by the

effective section modulus of the glass. Further complicating this study, the process of making the hole may introduce defects in the glass that affect its strength. Contact between the point support hardware and the glass may create additional stress concentrations as well. The subject of this research is the interacting effects of the hardware, drilling defects in the glass, and stress concentrations at these holes.

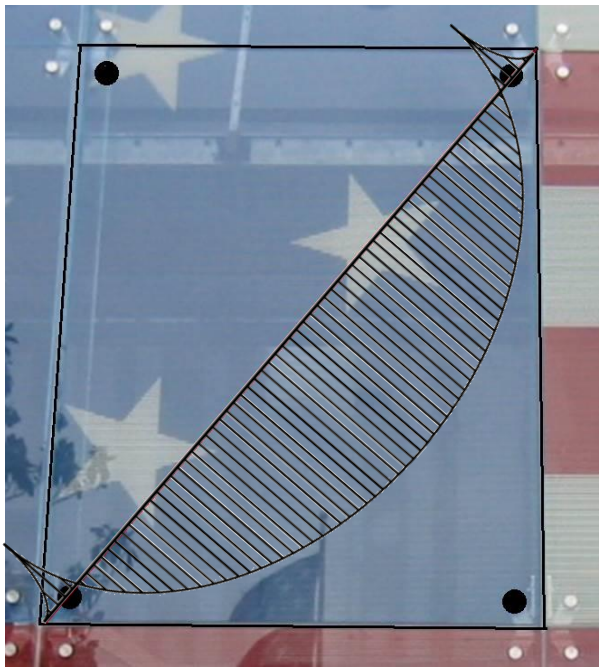

**Figure 9: Four-Point-Supported Glass Pane Behavior [10].**

## 1.3. General Information on Glass

Fully understanding the material properties of glass is key to successfully developing further theories on the strength of this amorphous material. This section reviews the current literature on glass properties that are most relevant to this research.

### *1.3.1. Glass Classification and Manufacturing*

Molecules of $SiO_2$, known as silica, which are obtained from pure sands, comprise the main structural units of glass [12]. During the manufacturing procedure, these construction units in the form of sand are mixed with other components and heated to their melting point ($2800^0$F) [12]. As the mixture cools, the construction particles of glass lose their transition mobility and become fixed in their position. They quickly develop their strength and material characteristics. These particles do not form any regular lattices within the glass structure, which is a characteristic property of amorphous materials. If these particles were formed in regular lattices (i.e., hexagons), they would be called crystals, and their material properties would be very different. The range of temperature at which these particles lose their mobility is called the transition temperature ($T_g$) [13]. The melting process of glass is reversible, which means that glass melts if heated again. This specific material property is very important for the tempering process discussed in Section 1.3.4, because during the tempering process, the glass material is heated up very close to its melting point at which glass behaves as a soft material.

Similar to all materials, the molecular composition of glass determines its mechanical and material properties. The admixtures added during the process of melting $SiO_2$ can change glass properties to get the desired glass behavior. Based on the ratio of admixtures added to $SiO_2$, commercially manufactured glass can be classified [14] as

- Soda-lime glass,
- Borosilicate glass,
- Lead glass,
- Fused glass,
- Silica glass,
- 96 percent silica glass.

In the structural glass industry, the two glass types most commonly used are soda-lime glass and borosilicate glass [14]. Soda-lime glass can be used to fulfill almost any architectural purpose, making it the more frequently utilized glass of the two. Borosilicate glass, on the other hand, is used only in instances where high temperature or chemical resistance is required [15]. Since this Master's project is focused on determining the strength of structural glass for most architectural purposes, it focuses on soda-lime glass. Table 1 summarizes the percentage content of ingredients in both soda-lime and borosilicate glass.

**Table 1: Glass Ingredient Content [16, 17].**

| **Components** | **Soda-lime silicate glass** | **Borosilicate glass** |
|---|---|---|
| $SiO_2$ | 69 – 74% | 70 – 87% |
| CaO | 5 – 12% | - |
| $B_2O_3$ | - | 7 – 15% |
| $Na_2O/K_2O$ | 12 – 16% | 0 – 16% |
| MgO | 0 – 6% | - |
| $Al_2O_3$ | 0 – 3% | 0 – 8% |
| Others | - | 0 – 8% |

It is also crucial to understand the manufacturing process. Glass manufacturing is a complex process that differs slightly from manufacturer to manufacturer, and each has their own secret for obtaining the highest quality glass. However, the general process is described as follows. Silica sand and glass admixtures ($Na_2CO_3$, $CaCO_3$, and others) are melted together in a furnace tower at temperatures of 2730 to $2820^0$F [12]. Once all the ingredients are melted together, molten glass is slowly cooled to a temperature of approximately $1830^0$F and poured on top of a tin bath, which causes the liquid glass to float and become perfectly flattened due to gravity. Completely flat glass pieces are slowly cooled to $1100^0$F as they process through the tin bath. At a temperature of around $1100^0$F, the glass becomes solid. Cooled glass is then dragged through the annealing lehrs where glass pieces are reheated back to their transient temperature ($1100^0$F) and cooled down very slowly. This process removes any residual stresses from glass caused by thermal expansion [12]. At the end of this process, monolithic annealed glass with essentially no residual stresses has been manufactured. After the annealing process, the glass is cut into the desired pieces and stored for client distribution (see Figure 10).

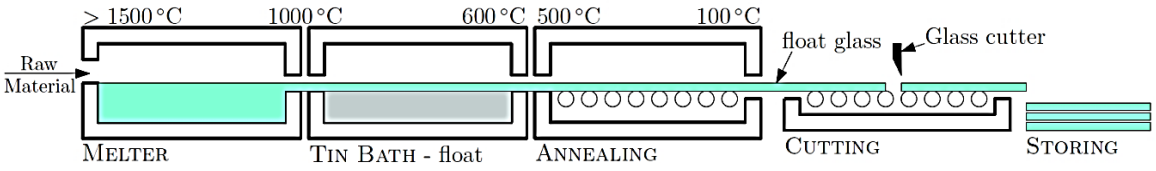


**Figure 10: Annealed Glass Processing [18].**

Monolithic glass can be subdivided into four subgroups depending on what type of treatment it receives after the initial manufacturing process. If no additional treatment is done, it is considered “annealed glass.” This type of glass is most widely used for glazing (except indoors and other high-traffic areas), glassware, and for any non-structural

purposes [19]. When annealed glass breaks, it shatters into many various-sized sharp pieces (see Figure 11). In contrast, additional treatment after the primary glass forming process creates “heat-strengthened” glass, “fully tempered” glass, or “chemically-strengthened” glass [19].

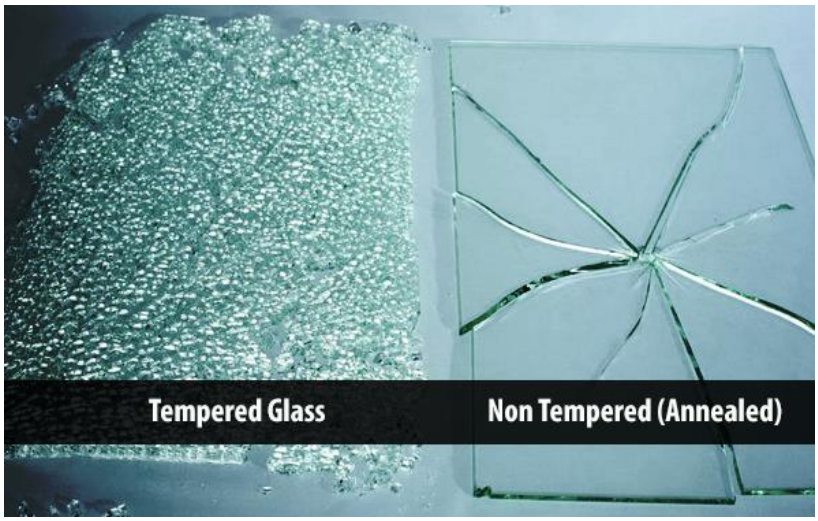


**Figure 11: Annealed and Fully Tempered Glass Breakage Patterns [20].**

The tempering treatment continues to further process the annealed glass (see Figure 12). The following description can be understood as a follow-up to Figure 10. Glass pieces must be cut and drilled according to any installation requirements before the tempering process can be continued since drilling, cutting, and any other shape-changing adjustments are not possible after glass tempering. The glass pieces are cleaned before entering the oven, where they are heated to their transient temperature ($1100^0$F) [13]. Soft glass pieces are cooled at a high cooling rate, which leaves the glass pieces with

tempering stresses. A more detailed description of glass behavior during the tempering process is described in Section 1.3.4.

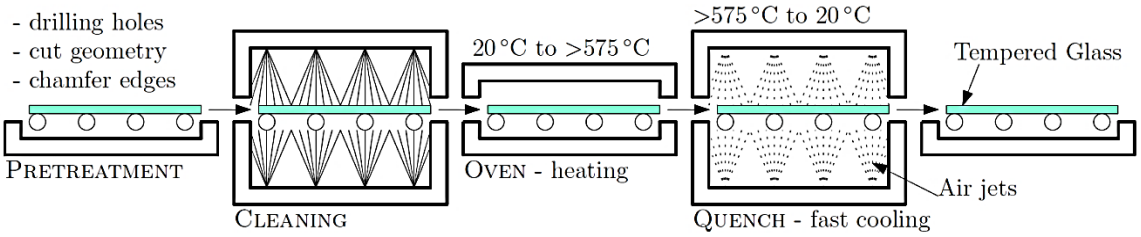


**Figure 12: Tempering Procedure [18].**

The main distinction between heat-strengthened glass and fully tempered glass is the extent of stresses the glass is tempered to. Per ASTM C1048 [21], compression stresses in heat-strengthened glass should range between 3500 to 7500 psi with no requirement for edge compression stresses. To be considered as fully tempered glass, it needs to develop a minimum surface compression of 10,000 psi and minimum edge compression of no less than 9,700 psi. A detailed description of the tempering process can be found in Section 1.3.4 of this report. The structural behavior of chemically-strengthened glass is improved by connecting alkali metal ions that are large in diameter (such as potassium) with the glass surface, which already contains small alkali metal ions (sodium ions). This contact induces an ion exchange that introduces compressive stresses on the surface layers of glass panes. Theoretically speaking, chemical strengthening can induce greater compressive stresses in glass than the tempering procedure [22]. However, in practice, high-level strengthening requires a considerable amount of time and money. Therefore, the extent of tempering is not as high as the theoretical value, and this type of glass treatment is not commonly used.

### *1.3.2. Mechanical Properties*

Similar to the manufacturing process, the mechanical properties of glass differ from manufacturer to manufacturer because the slight variance in ingredients marginally changes them. It has been shown that different ratios of $Na_2O$, $B_2O_3$, and $SiO_2$ vary the modulus of elasticity from as low as $E = 4760\ ksi$ to as high as $E = 12250\ ksi$ [23]. The American Architectural Manufacturers Association (AAMA) [24] establishes the average mechanical properties for soda-lime glass used in structural glass industry. The recommended values are summarized in Table 2.

**Table 2: Structural Glass Mechanical Properties [24].**

| Mechanical Property | Value | Units |
|---|---|---|
| E | 10,400,000 | psi |
| ν | 0.22 | - |
| ρ | 156 | $lb/ft^3$ |
| Tensile Strength of Annealed Glass | 5,800 | psi |
| Compression Strength of Annealed Glass | 120,000 – 145,000 | psi |
| Tensile Strength of Fully-tempered Glass | 17,400 – 29,000 | psi |
| Compression Strength of Fully-tempered Glass | 120,000 – 145,000 | psi |

### *1.3.3. Crack Growth and the Fracture Theories*

One of the biggest issues with glass is that its strength is greatly affected by microscopic cracks and flaws created during the cutting and/or drilling processes. Cutting and drilling processes are necessary procedures that take place during the manufacturing process, and unfortunately, these factors cannot be eliminated. When designing a glass structure, a designer must account for these imperfections and carefully decide on suitable drillings, edge finishes, and other procedures.

Theories regarding fracture mechanics on glass specify that the theoretical strength of glass can be as high as $4600\ ksi$ [25]. This value was estimated indirectly using Orowan's proposed theory that is based on the strength of the Si-O covalent bond [25]. What is known as Orowan stress is calculated by

$$\sigma_m = \sqrt{E\gamma/r_0}\ , \tag{1}$$

where $E$ is Young's modulus of elasticity, $\gamma$ is the fracture surface energy, and $r_0$ is the atom spacing of matter at equilibrium. General values for glass are (converted from SI units):

$$E = 10400\ ksi,$$

$$\gamma = 1.834\ x\ 10^{-6}\ BTU.in^{-2},$$

$$r_0 = 7.874\ x\ 10^{-9}\ inches.$$

Unfortunately, this is only a theoretical value and is difficult to achieve. In reality, this value is significantly lower depending on the manufacturing procedure. ASTM E1300 specifies that the design values for the edge strength of monolithic annealed glass is $2400\ psi$ and the edge strength of monolithic fully tempered glass is $10600\ psi$ [26]. This large strength difference was first described by Griffith [25] who tested glass and

found that the fracturing of glass does not start from the pristine surface, but rather from the imperfections and flaws within the glass introduced during the manufacturing process. He based his theory on energy equilibrium and stated that a crack is in a configuration that minimizes the total free energy of the system. He derived the Griffith energy-balance concept as

$$\sigma_f = \sqrt{2E\gamma/(\pi a_c)}\,, \tag{2}$$

where $\sigma_f$ is the failure stress, and $a_c$ is the critical crack length for crack growth determined experimentally [25].

His ideas were followed by Irwing who expanded upon the Griffith energy-balance theory and introduced the stress intensity factor K, which is oftentimes tabulated for different types of glass [25]. This factor reads as follows

$$K_I = Y\sigma_n\sqrt{\pi a}\,, \tag{3}$$

where $Y$ is a correction factor, $\sigma_n$ is the nominal tensile stress that is normal to the crack's plane, and $a$ is the crack size [25].

Unfortunately, these two theories are only applicable for sub-critical crack growth (i.e., growth due to corrosion or a steady load). In the case of force impact, a dynamic-like

fracture behavior has to be incorporated into the model. In a complex study, Mott incorporated the kinetic energy of a crack into the Griffith model and was able to predict the stress required for a crack to spread [25]. Since the microscopic flaws that determine strength are introduced during manufacturing and it would be impossible to measure every flaw, the most practical means of determining the strength of glass is through extensive testing.

### *1.3.4. Tempering Process*

Analogous to the prestressing of concrete beams and slabs in order to control surface tension in concrete, glass panes can be thermally treated to develop similar compression surface stresses to eliminate undesired surface tension. This process consists of two steps: a) slowly heating glass samples up to their transient temperature $T_g = 1100^0F$ and b) cooling them at a high rate [27]. Two phenomena occur during this two-step process.

First, since glass material below the transient temperature behaves as a solid with a positive coefficient of thermal expansion, its volumetric expansion is proportional to the positive change in temperature. As depicted in Figure 13 the thermal expansion of glass below the transient temperature can be linearly approximated with a line with a slope of $\alpha_1 = (13 - 90)\ \text{x}\ 10^{-6}/R$ [28]. The specified coefficient of thermal expansion for the soda-lime silicate glass is $CTE = 16\ \text{x}\ 10^{-6}/R$ [24]. Glass above the transient temperature expands at a different rate, but again can be approximated with a linear function with a slope of $\alpha_2 = (90 - 180)\ \text{x}\ 10^{-6}/R$ [28].

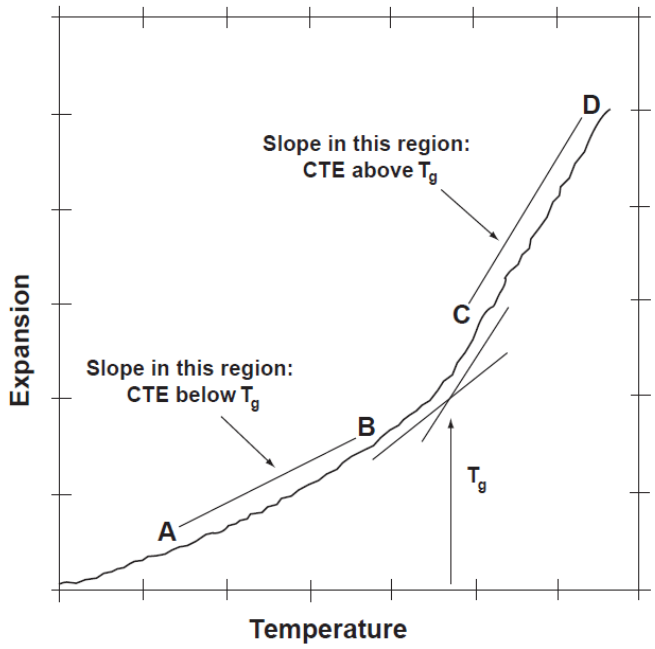


**Figure 13: Thermal Expansion of Glass [28].**

When considering a perfectly linear elastic material that has a finite thickness and is at temperature T, a high cooling rate creates a parabolic temperature gradient across its thickness. Since this material expansion is linearly proportional to its temperature, it consequently creates a parabolic stress gradient. This phenomenon can be illustrated as follows. As the temperature starts decreasing, the outermost layers of the material (the farthest from the central plane) cool while the inner layers remain at the original temperature. This temperature change makes the outermost layers contract while the inner layers are at the same volume experiencing compression forces. Subsequently, the temperature gradient creates tension stresses at the surface and compression stress in the central plane. Once the temperature gradient diminishes, no stresses are present. This

process is visually depicted in Figure 14. Perceivably, if glass behaved this way, it would not create any tempering. Furthermore, this temperature gradient creates tensile stresses in the material surface, which defeats the whole purpose of glass tempering.

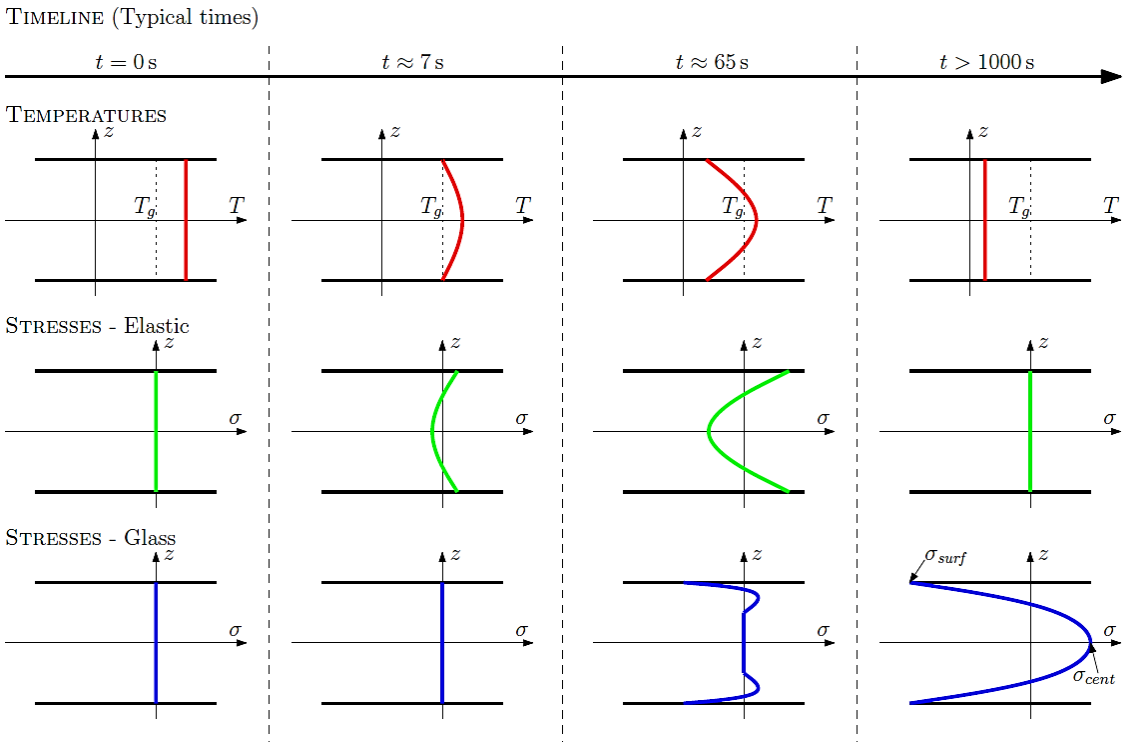


**Figure 14: Temperature and Stress Gradient over Thickness [18].**

The second and most important phenomenon is that glass behaves like a liquid at the transient temperature. Glass is between a "solid state" and "liquid state" at the transient temperature, and therefore, it can be seen as a "soft" material that is unable to develop any stresses. When the temperature starts decreasing below the transient temperature, the outermost layers of glass cool and contract. At the same time, they become solid while the innermost layers remain soft. At this point, the innermost layers do not exert any

stress on the outermost layers. Once the layers closer to the central plane cool down, they contract. Their contraction exerts compression stresses on the outer layers. As the material continues to cool even more, the innermost layers exert even more compression on the outer layers. Once the temperature gradient diminishes, these stresses persist. This tempering process is visually demonstrated in Figure 14.

It is noteworthy that the central plane glass layers are in constant tension. However, as Griffith described, the fracturing of glass does not start from a pristine surface [25]. Therefore, it is possible for glass to develop high tensile stresses at the central plane. Also, it is important to pay close attention to the edge effect. Tempering creates compression zones at edges of glass panes, which keeps cracks from opening. Nevertheless, if cracks are deep enough to spread to the tempering tensile zone, it can cause the glass pane to shatter.

### *1.3.5. Glass Lamination*

Glass may be laminated for structural use with two or more glass panes separated by a thin plastic interlayer. This interlayer adds extra physical properties to the laminated glass and increases its safety level over that of monolithic glass. Laminated glass acts as a composite material and has to be treated appropriately in analytical design.

The laminated glass procedure begins with a thorough cleaning of the glass layers to be laminated in an automated glass washer. After the cleaning, the glass enters an assembly room where the temperature and humidity are controlled. Here the interlayer is placed between two or more layers of glass sheets to be laminated. Any excessive interlayer is trimmed. Once assembled, a sandwich of glass sheets and interlayers passes through a

series of ovens and presses. First, the glass sandwich goes through an oven at $100^0$F, and immediately following, through a press that removes any air bubbles. Then, the glass sandwich continues to another oven where it is heated to the correct temperature depending on the thickness of the glass layers. Again, it passes through another press directly after coming out of the oven, where the edges are sealed. After this process, the glass sandwich is called glass laminate. To finalize the process, glass laminates are placed onto an autoclave where high pressure (160 psi) and a temperature of about $275^0$F perfectly bond the glass to the interlayer. The final step of the laminated glass procedure is the packaging and storing of the glass for delivery to clients [29].

The various types of laminated glass also have different specifications and advantages. Per ASTM C1172 [30], laminated glass can be composed of any of the types of monolithic glass described in Section 1.3.1. However, for glass with holes, fully tempered laminated glass is the most commonly used type for safety purposes [31]. Types of interlayers that bond two glass layers together vary depending on each manufacturer and the structural purpose of the specific laminated glass. Typical interlayers are PVB (polyvinyl butyral), ionomer, liquid resin, EVA (ethylene vinyl acetate), and polyurethane [32]. The PVB interlayer is the most common interlayer used by Stutzki Engineering, Inc. and is examined exclusively in this Master's project [31].

The advantage of laminated glass over monolithic glass is its improved post-breakage behavior. This means that shards remain a part of the glass pane and laminated glass keeps a certain minimal capacity to resist loads. Conversely, once monolithic glass reaches its ultimate stress, it is unable to sustain any further loading and fails. Monolithic annealed glass breaks into large sharp shards that are hazardous; monolithic tempered

glass breaks into pea-sized pieces. However, laminated glass is able to withstand minimal load demand after one or both layers reach their ultimate tensile stresses, and the shards remain a part of the glass pane minimizing endangerment. Figure 15 depicts characteristic post-breakage glass behavior. At Stage One, both layers carry the load experiencing bending stresses (if the interlayer has nonzero shear stiffness, compression in the top laminate and tension in the bottom laminate are superimposed onto the stresses shown in Stage One). When the bottom glass laminate breaks, the upper glass laminate can still carry some part of the bending demand (Stage Two). During testing, only 3 out of 30 laminated glass specimens demonstrated this behavior. The behavior at Stage Two is usually experienced when one of the glass plies breaks during improper handling during installation or when thermal breakage occurs. For quasi-steady loads (i.e., snow load), this behavior at Stage Two is not common. Stage Three behavior shows that tensile stress is carried solely by the interlayer and compression stress is carried by the broken upper glass layer. At Stage Three, laminated glass can barely resist any loads. The behavior improvement is that the interlayer secures glass shards, providing safety for users, and it nominally maintains the building envelope.

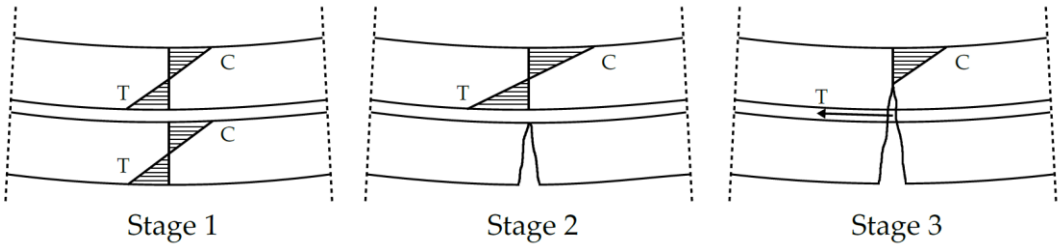


**Figure 15: Laminated Glass Post-breakage Behavior [33].**

### 1.4. Point-Supported Glass Literature Review

This section summarizes three research projects related to point-supported glass with respect to façades. The low number of research projects that have been conducted on the topic of point-supported glass illustrates the lack of available information. The first research project discussed in this section relates to monolithic fully tempered glass. The second and third focus on fully tempered laminated glass and its strength under out-of-plane loading.

The starting point for this Master's project was to look into the research carried out by Schneider and Worner at the Technical University Darmstadt in Darmstadt, Germany [34]. Schneider and Worner completed a study on glass breakage stresses in which they indicated different glass strengths for different cutting procedures. Monolithic annealed and monolithic fully tempered glass specimens of soda-lime and borosilicate glass were used. Each specimen type contained a hole drilled with three different methods, including

- Cylindrical hole with chamfer, diamond drilled;
- Countersunk conical hole with chamfer, diamond drilled;
- Cylindrical hole without chamfer, water-jet drilled.

In their research, they measured the tempering stresses in the middle of the specimens; however, they were unable to measure stresses at the hole's edge. Measuring tempering stresses right at the edge of a hole is not possible with current available technologies. The researchers used the tempering readings they did have, along with the available literature on tempering stresses, and calibrated their Finite Element Model. This Finite Element

Model was used to convert the axial force exerted on the coaxial double-ring test setup into stresses.

To examine the effect of tempering, they loaded both the annealed and tempered specimens to their ultimate failure. They reached the conclusion that the strength of annealed glass specimens is significantly dependent on crack size, which strongly correlates with the chosen drilling method. Schneider and Worner explained that the water-jet drilling method introduces the greatest number of flaws and the diamond drilling method creates the smallest cracks. They also found that tempering has a positive effect on the strength of glass because the compression stresses cover up the drilling cracks. They supported their conclusion with the observation that the water-jet drilled holes in annealed glass evince the lowest breaking stress due to the greatest amount of flaws. However, the breaking stress of water-jet drilled holes in fully tempered glass is comparable with the other drilling methods applied to the fully tempered glass. Their conclusion indicates that there is a healing effect in tempering that prevents the cracks from opening, and consequently averts premature glass failure. It also specifies that the size of defects from the drilling method has minimal influence on the strength of tempered glass.

No tests with the standard point-support fitting in place were conducted during this study. This leaves the unanswered question of how a fitting influences the strength of a glass pane. The fitting introduces another level of stress concentration that has to be taken into account during the design process. Also, no laminated glass specimens were tested. Therefore, this research project does not indicate a relationship between the strength of monolithic and laminated glass.

The second research project took place at Lund University in Lund, Sweden, an institution that has an extensive glass testing program in place. This study, conducted by Bength [35], investigated the effects of bolt fittings in fully tempered laminated glass. Bength utilized two different methods of testing to determine the capacity of cylindrical and countersunk fitting connections. First, a 20 x 20 inch square steel frame supported a specimen of the same size with a cylindrical and countersunk hole and corresponding fitting in place. For each fitting type, six replicates of a square 20 x 20 x ½ inch laminated specimen with a PVB interlayer were loaded normally by applying compression to the fitting. Due to the asymmetry of the countersunk fitting, compression force was applied to both sides of the fitting. The maximum breaking stress for each of the three loading cases is presented in Bength's research. It is unclear as to how the ultimate stress was calculated. The author of this Master's research project believes that the ultimate tensile stresses were determined based on two strain gauges placed very close to the edge of the hole at the tensile side of a glass specimen. Bength found that the maximum breaking stress (strength of glass) depends on the hole type and the fitting geometry. Table 3 summarizes Bength's published breaking stresses.

**Table 3: Bength's Discovered Breaking Stresses [35].**

| Loading Type | Mean Force (kN) | Mean Ultimate Stress (MPa) |
|---|---|---|
| Cylindrical Fitting | 4.61 | 177.13 |
| Countersunk Fitting – Compression Applied to Wider Side | 5.68 | 127.77 |
| Countersunk Fitting – Compression Applied to Narrower Side | 7.22 | 140.30 |

Bength utilized the Finite Element Model to evaluate the stresses in the laminated glass. She used the 3-D brick elements with radial meshing close to the hole. The Finite Element Model predicted higher stresses and lower displacements at the breaking load than the actual experimental values that she obtained. However, the key point of Bength's Finite Element Model is questionable because it predicts that the maximum principal stresses occur at the bottom of the first glass ply, which is bonded to the PVB interlayer. This is counterintuitive because one should expect the maximum principal stresses to be at the outer bottom surface of the laminated glass. This observation leads to the importance of properly modeled boundary conditions. Stutzki Engineering's method for modeling boundary conditions pays particular attention to this effect. As a result, no stress discontinuities will occur in the author's model.

In the second method employed by Bength, five 20 x 51 x ½ inch glass specimens with a cylindrical fitting in place were loaded via the fitting. The mean bending stress was determined for this loading type. Bength's finding is that the bending strength of laminated glass with a fitting is significantly lower than the compressive strength of laminated glass with a fitting in place. Her results are presented in Table 4.

**Table 4: Bength's Breaking Stress for Laminated Glass [35].**

| Loading Type | Mean Force (kN) | Mean Bending Moment (Nm) | Mean Ultimate Stress (MPa) |
|---|---|---|---|
| Cylindrical Fitting | 733.91 | 202.18 | 38.29 |

No comparison between the strength of laminated glass with a hole and the strength of laminated glass with a fitting in place was made. This leads to ambiguity when distinguishing strength reduction due to stress concentration caused by contact between the glass and the fitting.

The third research project also involved faculty from Lund University is the dissertation work of Froling [36] on the topic of strength design methods for laminated glass. This study examined the theoretical properties of laminated glass and the theoretical strength of laminated glass balustrades with 2 x 2 and 2 x 3 bolt patterns. The stress concentration was obtained from the FEM. Froling used an extensive Finite Element Model simulation and investigated different meshing possibilities of the laminated glass model. She compared the classical 3-D brick elements with 2-D shell elements. Based on her findings, Froling proposed the most appropriate meshing technique using the 2-D shell elements to improve the computation speed. Froling applied her theoretical data to create design charts for glass balustrades with two rows of bolts.

To verify her theoretical values obtained from the FEM, Froling used the experimental data from the previous research completed by Bength. Froling concluded that her proposed element type does not differ from the classical brick element types. However, both Finite Element Models predicted lower stresses than the experimental results obtained by Bength, which makes both of their results unimpressive. Table 5 summarizes Froling's presented results.

**Table 5: Froling's Comparison of Breaking Stresses for Laminated Glass [36].**

| Element Type | Maximum Principal Stress (MPa) |
|---|---|
| Experimental mean value (from Bength) | 177.1 |
| Proposed Elements (M-RESS) | 159.2 |
| Classical Brick Elements (C3D20R) | 153.4 |

As illustrated in the three studies above, the relevant and available literature demonstrates the need for more research on glass behavior under various loads and with various types of support. The lack of research and code support, as well as low confidence in the strength of glass with a drilled hole, prevents designers from exploring the full potential of point-supported glass.

### 1.5. Specific Statement of Objectives

The objective of this research project was to investigate the stress distribution near holes in tempered glass subjected to out-of-plane bending, as well as to determine whether strength is affected by hole drilling techniques and the presence of connection hardware in the hole. Stress distribution was studied by comparing classical plate solutions, FEA results, and measurements obtained through strain gauges placed on several specimens. A sub-objective of the project was to determine the appropriate stress concentration factor to use with a simple calculation of stresses on gross or net section properties. Strength was measured by testing plain (no hole) specimens subjected to four-point bending, and specimens with holes subjected to four-point and three-point bending. Three-point bending was achieved by loading the specimen with a standard cylindrical fitting in the hole.

There were two secondary objectives of this project. The first was to compare the strength of laminated and monolithic fully tempered glass. The second, to define how well the industry-standard procedure predicts strength combining an “equivalent thickness” with appropriate stress concentration factors.

# 2. STRESS CONCENTRATION FACTORS FROM PLATE THEORIES

An essential part of any building is its bearing system consisting of various structural members. These structural parts can transfer axial, shear, or bending forces into the ground. Depending on their position within the structure, their dimensions, and the set of forces they have to carry, these members can be classified as beams, columns, plates, shells, or membranes. Membranes are large, flat members resisting in-plane stresses only. Shells resist loads by generating in-plane stresses, as well as transverse shear and bending stresses. Glass structural members are most often flat, large members assumed to be subjected to out-of-plane pressure in the form of wind or snow load. In some applications, they are also subjected to point force caused by occupant live load. The best representation of such glass structural members is a plate model. Plates resist transverse loads by generating bending and shear stresses. Plate models can be categorized into three groups:

a) Thin Plates with Small Deflection,

b) Thin Plates with Large Deflection,

c) Thick Plates.

The difference between thin plates with a small deflection and thin plates with a large deflection is the magnitude of the deflection. When the deflection of thin plates approaches the order of the thickness of a plate, in-plane tensile stresses (i.e., the membrane action) that were negligible in the case of small deflections become large enough to alter the bending stresses. Thin plate theory with a large deflection that accounts for this effect must be used. The difference between thin plate theories and thick

plate theories is that thick plate theory includes shear deformation [37]. This study assumes that deflections of the tested glass specimens are relatively small, so thin plate theory with large deflection was not explored. The following sections describe the difference between thin plates with small deflections and thick plates in more detail.

In addition to the abovementioned theories, stress concentrations around holes in plates play a key role in this study. A hole for a fitting in each of the four corners of a glass pane creates an obstruction for stress flow that has to be overcome. Stress flow must go around such obstructions, which creates zones of higher stresses. Some of the classical theories derive the stress concentration factors for an infinite plate. According to Timoshenko [37], there is very little difference between infinite and finite width plates as long as the width of the hole remains small compared with the overall dimensions of the plate. The oldest classical theories define the stress concentration factor as a ratio of the peak stress to the stress applied in the far field, using gross section properties away from the hole [37]. However, newer stress concentration publications define the stress concentration factor as the ratio of the peak stress to the average stress in the effective cross-section at the hole [38]. This means that the cross-sectional area of the hole is subtracted when calculating the section modulus. For the purposes of this study, $K_{gross}$ is the stress concentration factor calculated using the gross section properties, whereas $K_{net}$ is the stress concentration factor calculated with net section properties.

### 2.1. Stress Concentration Factors for Thin Plate Theory

This section is a summary of material presented by Timoshenko [37]. Thin plates can be modeled as two-dimensional objects with no assumed thickness. The plates are modeled

by the mid-surface, which is a section taken in the mid-thickness of a very thin plate. The assumptions related to this simplification are:

a) There is no deformation in the middle plane of the plate. This plane remains neutral during bending.
b) The points of the plane lying initially on a normal-to-the-middle plane of the plate remain on the normal-to-the-middle surface of the plate after bending.
c) The normal stresses in the direction transverse to the plate can be disregarded.

One can see that these assumptions follow the small deflection restrictions for thin plates. Since the plate is thin, the rotation of its cross-section is small, and all points remain perpendicular to the mid-surface before and after deformation takes place. Since the deflections are very small, there are no lateral deformations caused to the mid-surface of the plate. There is also no significant in-plane stress that would affect the bending stresses due to the minimal magnitude of the deflections. Based on these assumptions, all stress components can be expressed by the plate deflection function $w(x, y)$ with two coordinates. This function must satisfy a linear partial differential equation for displacements together with the boundary conditions.

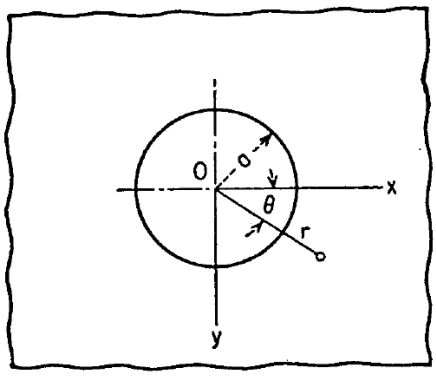


**Figure 16: Radial Coordinates [37].**

Since the holes in the plates are circular in shape, Cartesian coordinates $x, y$ were used and easily converted to radial coordinates that better describe stress around a hole. With radial coordinates, each point is fully defined by a radius and angle (see Figure 16). A deflected

shape function $w(r,\theta)$ must satisfy the boundary conditions; the resultant moments can then be derived from the general plate relation between the deflected shape and moments. The solution for a uniaxial bending around the y-axis is

$$M_t = M_0\left[1 - \frac{2(1+\nu)}{3+\nu}\cos 2\theta\right]. \tag{4}$$

The moment $M_0$ is the uniaxial bending moment applied at the far edges of a plate. The maximum moment, which causes the maximum stress, occurs at $\theta = 90°$. At this location, $M_t$ is $M_y$. This maximum is

$$M_{y(\max)} = \frac{5+3\nu}{3+\nu}M_0\,, \tag{5}$$

and the gross stress concentration factor is

$$K_{gross} = \frac{M_{y(\max)}}{M_0} = \frac{5+3\nu}{3+\nu}. \tag{6}$$

Glass has Poisson's ratio $\nu = 0.22$, and when substituting this value into the stress concentration formula, Equation (6) for thin plates results in $K_{gross} = 1.758$.

## 2.2. Stress Concentration Factors for Thick Plate Theory

In review, one of the assumptions about thin plates is that a cross-section remains perpendicular to the deformed mid-surface (the mid-surface for a plate is comparable to the elastic curve for a beam). This assumption disregards transverse shear deformation. In thin plate theory, the shear deformation energy is not included in the energy equation. When a cross-section becomes thick enough, it is no longer acceptable to ignore shear deformation, and the cross-section does not remain perpendicular to the mid-surface. This phenomenon is depicted in Figure 17. The limit for when the shear deformation becomes significant is based on the thickness to span ratio. Plates with a thickness to span ratio greater than 1/20 are considered thick plates, whereas plates with a ratio smaller than 1/20 are classified as thin plates [39].

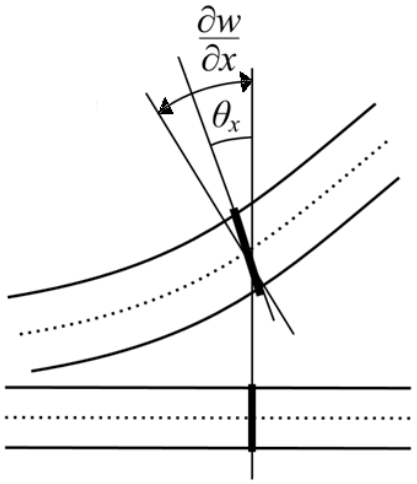


**Figure 17: Shear Rotation of Plates.**

When the one-way bending of plates without any holes occurs, there are no shearing stresses, and the thick plate model coincides with the thin plate model. Consequently, test specimens without a hole loaded using the four-point-bending test setup will not experience any transverse shear deformation in the constant moment region.

However, shear stress and the corresponding deformations become significant in locations of bending-stress concentrations. Specimens with a hole in the constant moment

region must redistribute the moments around the hole. This moment redistribution along the cross-section is accompanied by shearing stresses based on the formula $V(x) = EI\frac{\partial M}{\partial x}$. Therefore, the shear stresses in the area around the hole become very high, and should be accounted for in the stress concentration calculations [40].

The inclusion of shear deformations in calculating the stress concentration factor was first introduced by German-American mathematician, Eric Reissner, and were observed in the FEA portion of this study. Riessner proved that the shear stresses are non-zero in the region near the hole, and reach their maximum at 45 degrees to the plate's primary axes.

According to the thick plate theory that includes the shear deformations, Reissner's stress concentration factor [41] is

$$K_{gross} = \frac{3}{2} + \frac{1}{2}\frac{\frac{3(1+\nu)}{2}K_2(\mu) - K_0(\mu)}{\frac{(1+\nu)}{2}K_2(\mu) + K_0(\mu)}, \tag{7}$$

where

$$\mu = \frac{d\sqrt{10}}{h}, \tag{8}$$

and

$d = hole\ diameter,$

$h = plate\ thickness,$

$K_n(x) = Bessel's\ functions\ of\ n - th\ order.$

For this specific study, the glass specimens with Poisson's ratio $\nu = 0.22$, width $8\ inches$, and thickness of $0.485\ inches$, the stress concentration factor is $K_{gross} = 1.947$.

### 2.3. Discussion on Thick and Thin Plate Theories

The difference between stress concentration factors predicted by thin and thick plate theories is 10%. This also means that when the applied moment and resultant far-field bending stress are known, the peak stress at the edge of a hole predicted by the two theories will differ by 10%. This significant difference is attributed to the shear deformation that is omitted in thin plate theory. Based on the FEA results, the more realistic plate theory was chosen for this research project.

### 2.4. Peterson and Roark Stress Concentration Factors

A very popular engineering resource for calculating the stress concentration factor is the publication *Roark's Formulas for Stress and Strain* (Roark) [38], which incorporates work from *Peterson's Stress Concentration Factors* (Peterson) [42]. Both of these publications collect stress concentration factor theories from various authors for various loading conditions and reformat them into more user-friendly equations. Since both works provide two very similar equations that lead to the very same stress concentration

factors for out-of-plane uniaxial bending of *finite* width plates, Roark is the only theorist discussed in this section. The equation provided by Roark is

$$K = \left[1.79 + \frac{0.25}{0.39 + \left({}^{2r}/_{t_p}\right)} + \frac{0.81}{1 + \left({}^{2r}/_{t_p}\right)^2} - \frac{0.26}{1 + \left({}^{2r}/_{t_p}\right)^3}\right]\left[1 - 1.04\left(\frac{2r}{H}\right) + 1.22\left(\frac{2r}{H}\right)^2\right]. \quad (9)$$

In contrast to finite width plate theories, the drawback of Reissner's stress concentration theory for thick plates is that it assumes the plate has an infinite width during the derivation. For the four-point-bending test setup, different plate width FE models were constructed while the hole diameter $d = 1.428\ inches$ and plate thickness $t_p = 0.485\ inches$ remained constant. Particularly, plates of width $H = 20, 10, 8, 5,$ and $4\ inches$ were examined. It was discovered that Reissner's stress concentration requires a limit of $\frac{H}{d} > 5.6$ to be an accurate prediction of the peak stress at the edge of a hole. For the tested glass specimens with the width of $H = 8\ inches$ and hole diameter of $d = 1.482\ inches$, this condition is met. It is also noteworthy that it is common practice to place a corner fitting $4\ inches$ away from both corner edges for both aesthetical and construction purposes. Therefore, Reissner's theory is applicable to this practice. However, the ASTM C1048 code allows the fitting to be $3/4\ inch$ close to the edge for a $1/2\ \ inch$ thick plate, which results in a plate as narrow as $H = 3\ inches$. For these borderline cases, Reissner's theory is not applicable, and the stress concentration theory for finite width plates must be used.

Using Equation (9), the net section stress concentration factor that is used in the experimental data, Section 4.3.4, is $K_{net} = 1.654$ for monolithic glass specimens and $K_{net} = 1.537$ for laminated glass specimens. The stress concentration factor for laminated glass is based on the average thickness of all bottom glass plies $t_{BOTTOM} = 0.225\ inches$ and the all bottom hole diameters $d_{BOTTOM} = 1.654\ inches$.

Roark provides the net section stress concentration factor for finite plate width without referencing the original author. It is assumed that the net section concentration factor for finite width plates provided in Roark is a reasonable approximation to the original theory.

# 3. FINITE ELEMENT MODEL

Another method for investigating the stress concentration around a hole in glass specimens is modeling a representative glass specimen using the Finite Element Model. For the purposes of this research, the finite element program Abaqus was used [43]. Abaqus is a commercial software used by many structural companies including Stutzki Engineering, Inc. for modeling structures and complex details.

Within Abaqus, there are several model options available for modeling structural glass specimens. The two most appropriate options are using shell elements or three-dimensional solid elements. The shell model follows the classical mathematical plate theories and is a two-dimensional representation of a glass specimen. If one was to use the shell model, the advantage is the high computational speed at which calculations can be processed. The other option is to model a glass specimen using three-dimensional solid elements. This is the preferred method for glass element simulation at Stutzki Engineering, Inc. Both, the monolithic four-point-bending and monolithic three-point-bending specimens, were modeled with solid elements using Abaqus. The laminated specimens were not modeled in this research.

## 3.1. Geometry and Material

The FEA model's geometry and material need to represent the actual specimen as accurately as possible. The author of this study has not attempted a comprehensive sensitivity analysis or comparison of the various options for FEA; rather, the standard office procedures of Stutzki Engineering, Inc. were followed as closely as possible.

The dimensions of the modeled glass specimens were length $L = 16\ inches$, width $b = 8\ inches$, and thickness $t = 0.485\ inches$. The hole diameter of the glass specimen was $d_h = 1.428\ inches$. To simulate the loading conditions as accurately as possible, the loading and bearing edges of the test setup were modeled as well. This was accomplished by modeling solid steel bars that represent the edge of both the loading and bearing edges. The loading and bearing edges were centered with regard to the center of the hole. The bearing edges were $s_b = 8\ inches$ apart, and the loading edges span was $s_l = 14\ inches$, as was the case in the actual test setup. The diameter of the solid bars also followed the actual dimension of the test setup and was $d_b = 0.250\ inches$. The length of each bar was $L_b = 8\ inches$. Monolithic glass specimens were assumed to be made of perfectly linear-elastic material. The modulus of elasticity was assumed to be $E = 10{,}400{,}000$ psi with Poisson's ratio $\nu = 0.22$. It was also assumed that loading occurs at room temperature 69°F and over a short enough period of time that there were no viscoelastic effects. The bearing and loading edges were modeled with stainless steel linear-elastic material. The modulus of elasticity was $E = 29{,}000{,}000$ psi and Poisson's ratio was $\nu = 0.30$.

### 3.2. Mesh

Mesh selection plays a significant role in obtaining accurate results. Inappropriate size, shape, and distribution of elements can alter the results and stress distribution, which are important in determining local zones of stress concentration. The general rule states that the more elements, the more accurate the results. However, solutions for an increasing number of elements per specimen converge. Consequently, at some point meshing glass specimen with a finer mesh does not notably alter the stress values and stress distribution.

It was experimentally determined with the four-point-bending simulation that elements with a size of 0.17 x 0.17 $x$ 0.121 $inches$ (width x length x height) resulting in 4 elements per thickness, 46 elements in width, and 98 elements in length converge to accurate results. Linear hexahedral elements (C3D8I) were used. Based on this element type, the most accurate results are obtained if all sides of the element are perfectly square. Therefore, in this study radial distribution of the element was used around the hole to get as close to the cubic shape as possible (see Figure 18).

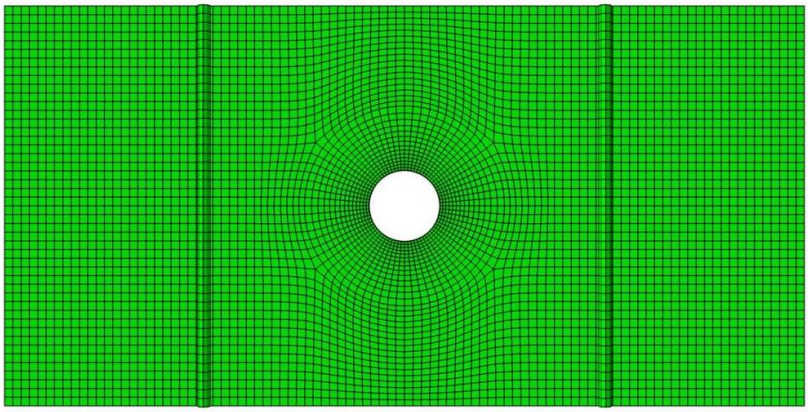

**Figure 18: Monolithic Glass Specimen Meshing.**

### 3.3. Interaction Properties

Experiments with the FEA four-point-bending simulation determined that restraining elements that form a bearing edge from movement in the direction of the load creates stress discontinuity and varies the peak bending stress. To eliminate this effect, the actual bearing edge and related interaction between the bearing edge and specimen must be modeled. It is also a common practice of Stutzki Engineering, Inc. to model the actual fittings to create boundary conditions that are as realistic as possible. Part of modeling the actual bearing edges is defining the contact between the bearing edge and glass specimen.

Per Stutzki's recommendations, Abaqus' "contact pair method" was used to define the contact between the loading or bearing surfaces and the glass. In this method, the slave surface and master surface are assigned. The slave surface is the bigger and weaker surface compared to the master surface, which is the stiffer and harder surface. In this research project, glass surfaces were assigned to the slave surface, and the loading and bearing edges were assigned to the master surface. Contact stiffness between these two was set to be linear, which complements the linear behavior of both materials. The built-in function of surface smoothing was used to allow for better solution convergence. The friction coefficient between glass and steel was assumed to be $\mu = 0.1$.

### 3.4. Load and Supports

The representative load of 500 lbf was applied through the reference point to each loading edge resulting in 1000 lbf total force applied. This was accomplished using a coupling constraint between a reference point and both top surfaces of the loading edges. This coupling constraint works as a lock between members, forcing them to move and act together. If the load is applied to the reference point, it is evenly redistributed to the loading edges through the coupling restraint. If the reference point moves in one direction, the loading edges move accordingly.

Support boundary conditions were formed by preventing the translation of certain members. The bottom surfaces of the bearing edge were restrained from vertical (z-direction) translation. Two stabilizing points were used to simulate the floating conditions of a glass specimen. One corner of the specimen was restrained from translation in both horizontal directions (x and y directions), and the other corner was restrained from

movement in the y-direction only. This fully and completely defines and restrains all possible degrees of freedom of the glass specimen.

### 3.5. Results

Once the analysis was performed, the resulting stresses and displacement were displayed in the Abaqus preview mode. Abaqus allows users to view in-plane stresses, maximum principal stresses, Mises stresses, and several other types of stress. Abaqus designates the in-plane stresses with the letter "S." The S1 stresses are the stresses applied along the x-axis and represent the resultant bending stresses caused by the total 1000 lbf applied force. Figure 19 and Figure ***20*** show the distribution of theoretical bending stresses in a glass specimen.

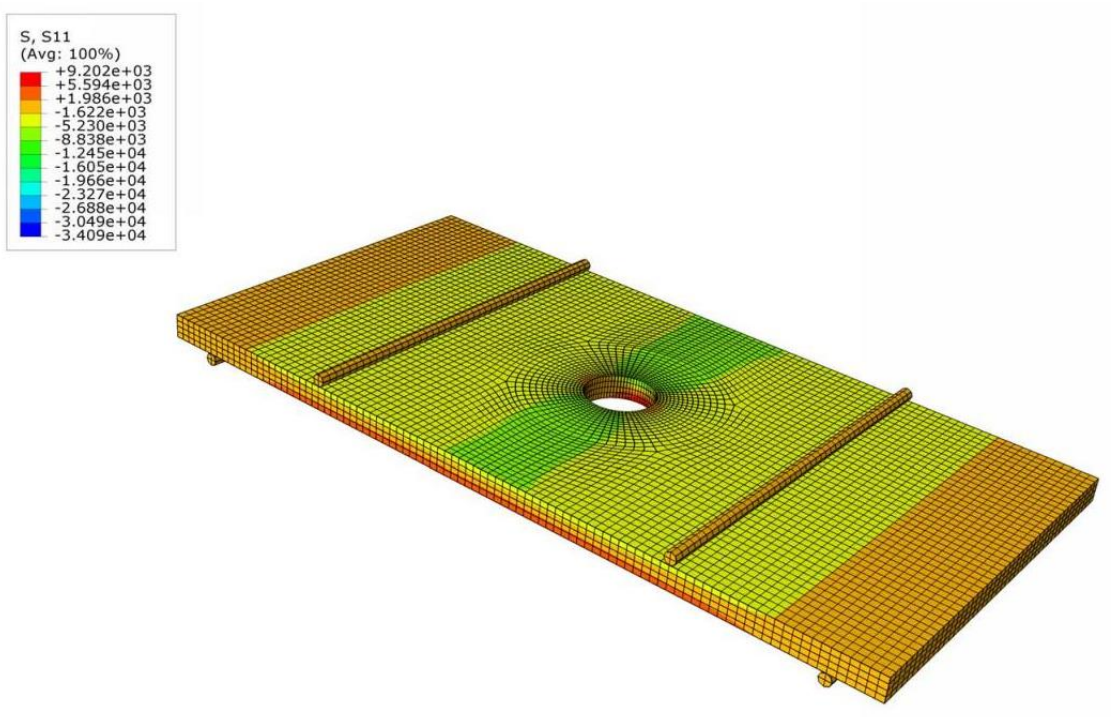


**Figure 19: In-plane Bending Stresses – Top Surface.**

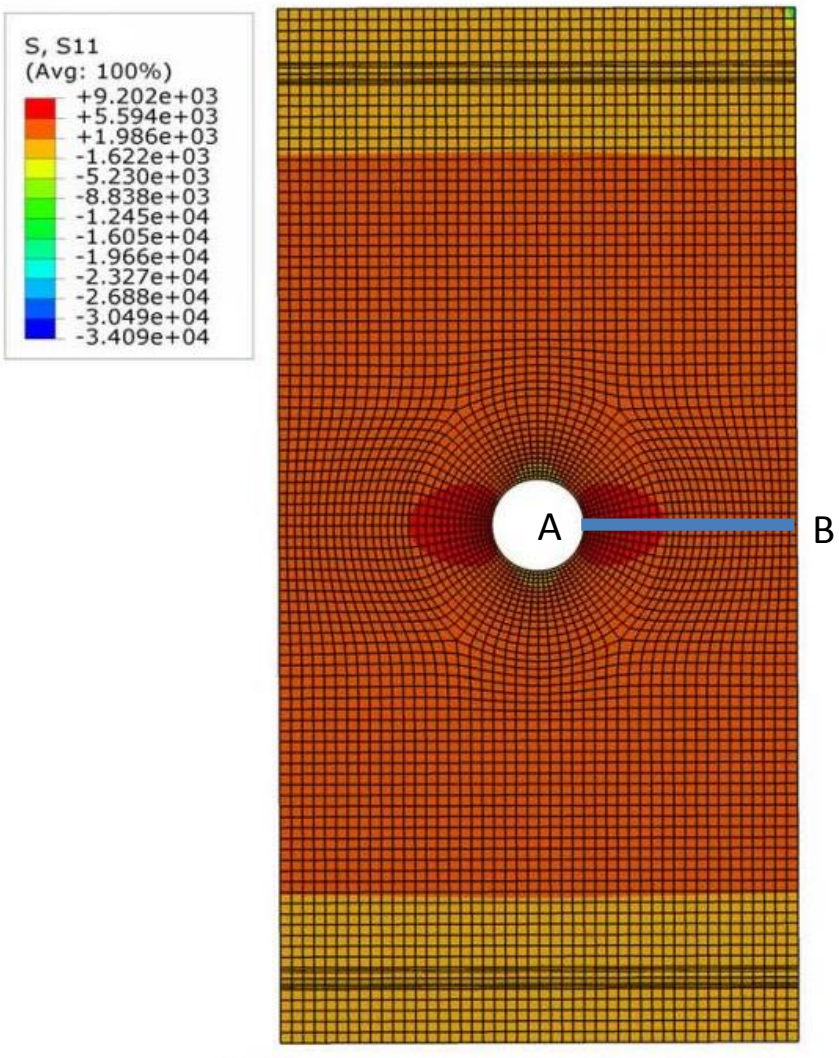


**Figure 20: In-plane Bending Stresses – Bottom Surface.**

Figure 21 depicts tension stresses S1 on the very surface versus the distance from the edge of the hole. The glass specimen experiences these stresses as if a section plane was cut through points A and B, as displayed in Figure 20. The green dotted line in Figure 21 represents the average stress level across the net section of the glass specimen. The value of the unaffected stress is $\sigma_{net} = 5785$ psi. The blue dotted line represents the stress

gradient on the line AB. The peak stress value is $\sigma_{peak} = 9202$ psi. The corresponding stress concentration factor is calculated as

$$K_{net} = \frac{\sigma_{peak}}{\sigma_{net}} = \frac{9202}{5785} = 1.591. \quad (10)$$

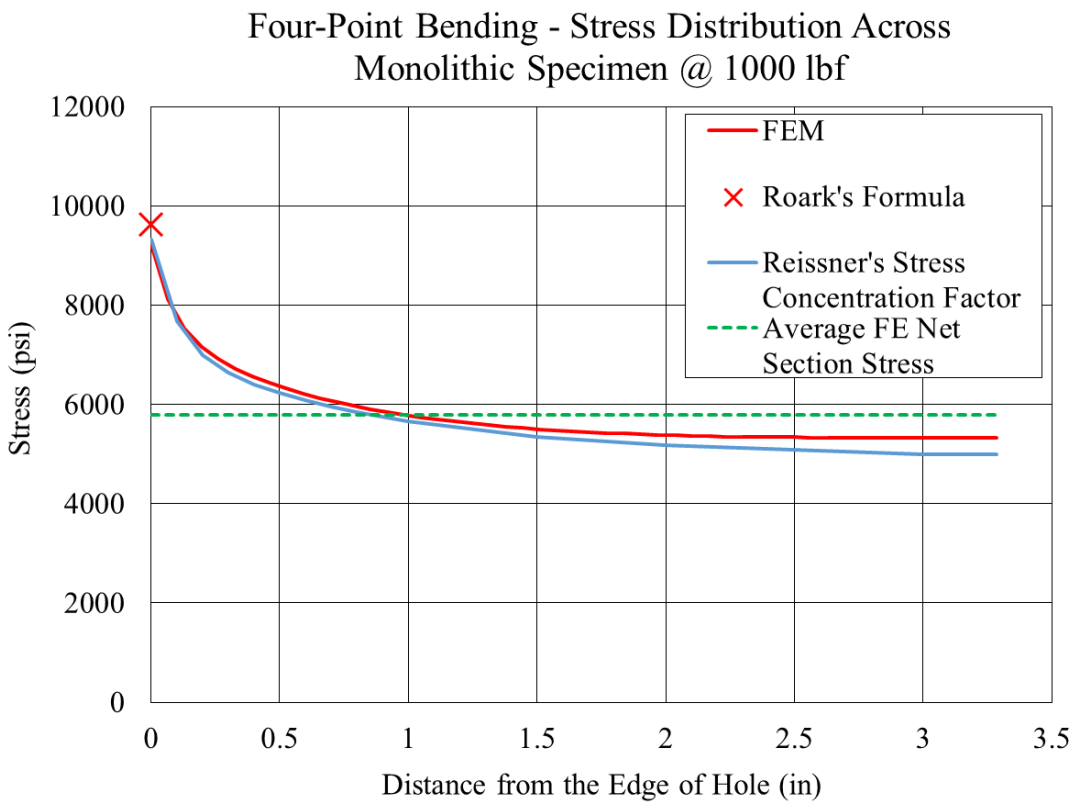


**Figure 21: Stress Concentration Factor Comparison.**

### 3.6. Comparison of Stress Concentration Factors

Table 6 compares the peak stresses predicted by Reissner's theory, the Roark reference, and the Abaqus model.

**Table 6: Stress Concentration Factor Comparison.**

| Plate Width | $\sigma_{peakABAQUS}/\sigma_{peakROARK}$ | $\sigma_{peakABAQUS}/\sigma_{peakREISSNER}$ |
|---|---|---|
| 4 in Wide Plate | 92.1% | 111.8% |
| 5 in Wide Plate | 94.1% | 105.3% |
| 8 in Wide Plate | 95.5% | 98.8% |
| 10 in Wide Plate | 96.2% | 98.0% |
| 20 in Wide Plate | 98.4% | 98.3% |

Both the Roark and the Reissner stress concentration factors are acceptable predictions for plates with 8 inches or greater width, and neither is appropriate for plates with a width of 4 inches or less. Because the calculation of the Roark stress concentration factor is much simpler than Reissner's, the Roark stress concentration factor is used in the remainder of this paper.

# 4. EXPERIMENTAL TESTING

## 4.1. Specific Objectives of Each Set of Tests

### *4.1.1. Monolithic Specimens*

Each specimen type represents a specific loading situation and isolates variables to allow for a separate assessment of each loading effect.

Type 4N (4-point bending, no hole): The main purpose of testing plain monolithic glass specimens without holes loaded four-point bending was to determine the basic tempered glass pane strength and to serve as a base for comparison with other specimen types.

Type 4H (4-point bending, with hole): Monolithic glass specimens with a standard water-jet drilled hole loaded four-point bending reveal the strength of tempered glass near the hole in a glass sheet. The water-jet drilling process creates little chips and microscopic flaws near the edge of the hole, and any reduction in strength of these specimens may be attributed to these flaws.

Type 3H (3-point bending, with hole): The purpose of monolithic glass specimens with a standard water-jet drilled hole loaded via a standard swivel fitting was to determine whether there is a strength reduction caused by the swivel fitting itself. The way the swivel fitting pushes against a glass specimen over a small area creates local stress concentrations, which could affect the failure. When the strength of specimens loaded via a fitting is compared to that of specimens with holes loaded four-point bending, any strength reduction may be assumed to arise from the fitting contact and may be classified as net strength of a glass pane with a fitting.

Type 4HP (4-point bending, with hole, with extra chamfer of hole edge): A set of monolithic glass specimens with additional hole edge chamfering was loaded four-point bending. Comparing the results of these specimens with those of the 4H specimens can indicate whether manufacturing details have a significant effect on strength.

### *4.1.2. Laminated Specimens*

Laminated glass specimens were also tested. Industry-standard procedures for calculating equivalent section properties for laminated glass were used to calculate stresses in the laminated specimens. Discussion of the comparison between monolithic and laminated glass specimens is provided in Section 4.3.4. It was predicted that the breaking stress was going to be the same for both monolithic and laminated specimens since all glass sheets are made of fully tempered glass.

Type 4NL (4-point bending, no hole, laminated): These provide a base strength for laminated glass.

Type 4HL (4-point bending, with hole, laminated): This strength was compared to that of the 4NL specimens. Any differences in strength could be attributed to the hole effect and microscopic flaws from the drilling process.

Type 3HL (3-point bending, with hole, laminated): Laminated glass specimens loaded via a fitting were tested to observe the influence of the contact between the fitting and the laminated glass specimen.

No laminated glass specimens with chamfered hole edge were tested.

## 4.2. Experimental Test Setup

### *4.2.1. Test Setup and Testing Procedure*

Two distinct mechanisms were used to determine the strength of the glass specimens: a four-point-bending test setup and a three-point-bending test setup. The four-point-bending test setup created a constant moment region with no shear between two loading points. This type of loading was used to determine the pure bending strength of the glass specimens. The three-point-bending test setup was utilized to evaluate the effects of a fitting. Each glass specimen was placed on the exact same base with two bearing edges and was loaded directly through the fitting.

Both test setups follow the key recommendations of the ASTM C158-02 that specifies requirements for the determination of the strength of glass by flexure [44]. The standard four-point-bending test setup consists of the bearing and loading parts, as shown in Figure 22. The bearing part is fixed to the compression bench and creates a support for the specimens. The distance between bearing edges is $14\ inches$. These bearing edges are made of steel angles with a bearing edge radius of $1/8\ inches$ and are fixed to the bearing plate. The connection of angles to the bearing plate is provided through bolts. Slotted holes in the bearing plate provide full adjustability to the bearing edges. The bearing edges are covered with $0.06\ inches$ thick delrin – very hard plastic – to prevent any hard contact between steel and glass. The loading part consists of a loading plate, loading edges, and a swivel fitting. The loading edges are made of steel angles and bolted to the loading plate. In the same way as the bearing plate, slotted holes in the loading plate are provided to secure full adjustability of the bearing edges. The loading edges are covered with delrin as well and span $8\ inches$. In the exact center of the loading plate,

there is the swivel fitting that holds the loading plate and allows it to move and adjust to any imperfections of the glass specimens. Therefore, the loading part is fully able to pivot and does not create any moment in a loaded specimen. The swivel fitting is mounted to the load cell which is connected to the press. By rotating a manually operated wheel, a shaft connected to the load cell comes out and presses down on the loading part. The three-point-bending test setup (Figure 23) uses the same components with the absence of the loading part. The swivel fitting that is used for holding the loading plate is substituted with the same type of swivel fitting that directly clamps the glass specimens. Those glass specimens were loaded via the fitting that pushes the glass specimen against the bearing edges. This swivel fitting is a standard representative swivel fitting used in the glass industry for mounting standard glass panes to other components of a structure.

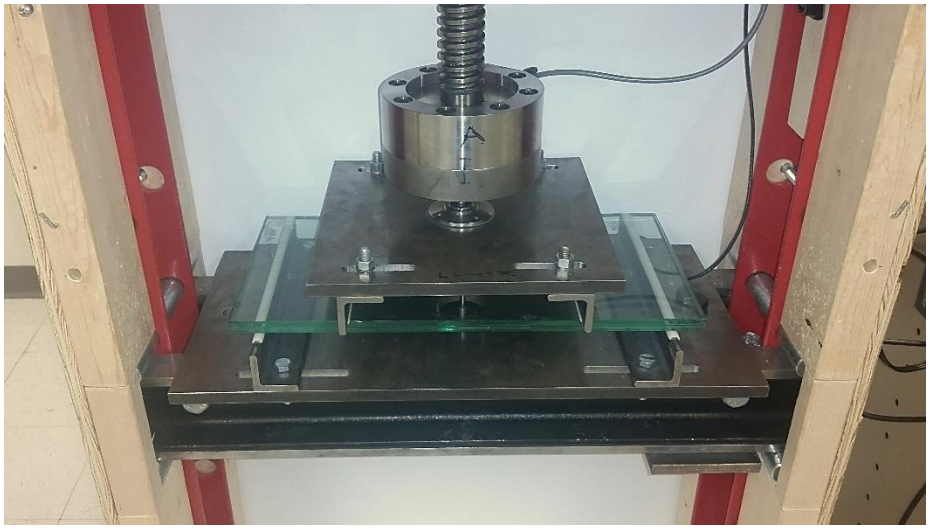

**Figure 22: Four-point Bending Test Setup.**

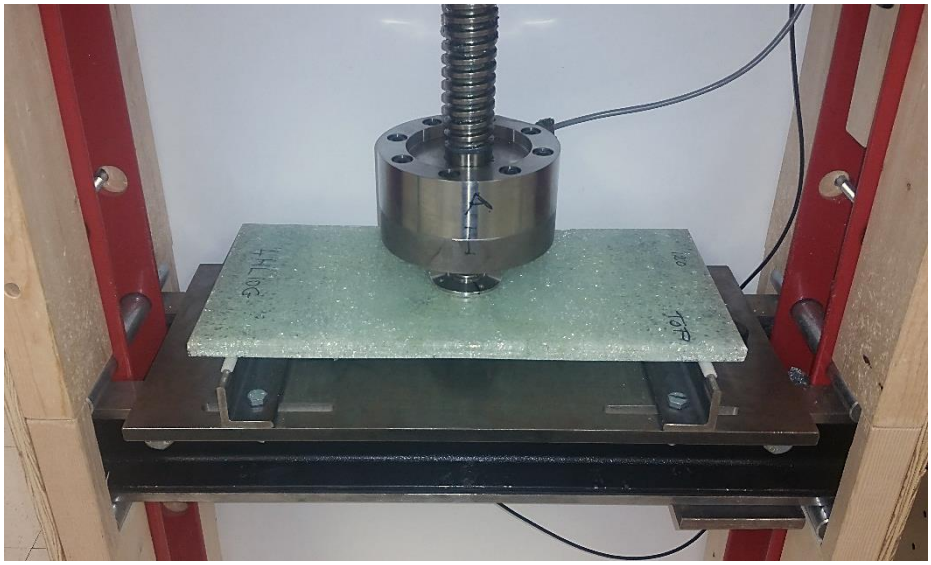

**Figure 23: Three-point Bending Test Setup.**

The test procedure included making careful measurements of the specimens, ensuring that each specimen was aligned in the test frame, and applying the load.

The load was applied by manually turning the crank on the test system, as shown in Figure 24. Each turn of the crank created a displacement of $0.033\ inches$. A constant displacement rate of $0.2\ inches/minute$ was achieved by maintaining a constant rate of 6 turns of the crank per minute. This was verified after tests by plotting the displacement reading from the linear variable displacement transducer (LVDT) versus time.

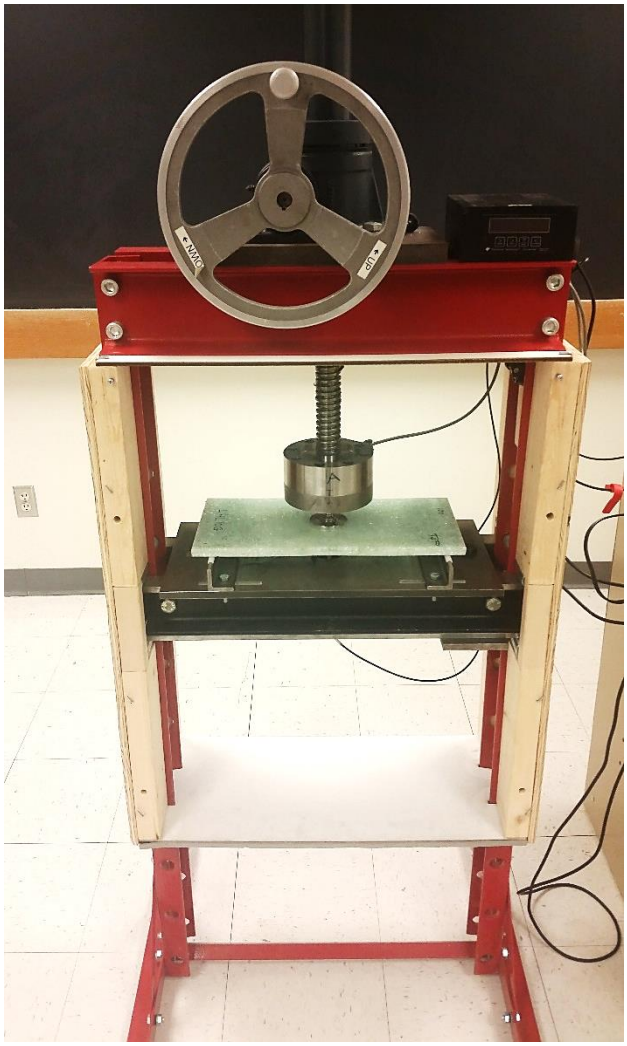

**Figure 24: Compression Bench.**

Load was measured by the strain-gauge load cell, Transducer Techniques model LPU-K with 15000 lbf capacity, operating with a matched signal conditioner, Transducer Techniques model DPM-3. Complete calibration of the load cell was last completed on March 19, 2013 by Transducer Techniques.

The linear variable displacement transducer (LVDT) is a device used for measuring linear displacements. Plastic brackets were used to tighten down the LVDT and clamp it to the

bottom side of the bearing plate. A circular opening in the center of the bearing plate allows the LVDT to vertically protrude through the bearing plate to the level of the bearing edges. When a glass specimen was placed on the bearing edges and deflected down under the pressure, the LVDT touched the bottom side of the specimen and read its vertical displacement right in the center of the specimen.

The S5-500AG LVDT by Honeywell was used. This LVDT's span is $\pm 0.5\ inches$, which allows for a $1\ inch$ total linear displacement range. Before the first run of tests, this LVDT was calibrated to read the most accurate values. The 762XFL-2 electronic caliper by Starrett, with a precision of $0.00005\ inches$, was utilized to calibrate the LVDT. Both measuring devices were firmly tightened down in a stand and pressed against each other. The readings in the linear displacement on the electronic caliper had to be equal to the linear displacement read on the LVDT.

The following readings were made:

$$5.00V = 0.5\ inches\ ,$$

$$-4.99V = -0.5\ inches.$$

Therefore, the overall error of measurements is less than $\frac{(5.00V+(-4.99V))}{10V}(100) = 0.1\%$. Additional verification of linearity was not done.

Strain gauges were FLA-3-11-5L from Tokyo Sokki Kenkyujo, Ltd. They were applied with ACE Super-Glue after careful measurement for alignment. Signal conditioning for the strain gauges was provided by a National Instruments SG-43 module.

Data acquisition was performed with a National Instruments CA-1000 coupled with a laptop computer. The data for each channel were recorded every $0.5\ second$.

### *4.2.2. Mockup Specimen*

A steel mockup specimen provides a basic way to check the test setup, LVDT, and strain gauge readings. A steel plate $16\ inches$ in length, $14\ inches$ in width, and $0.494\ inches$ thick served as a representative sample of a typical glass specimen. One strain gauge was applied in the very center of this steel specimen. A load versus strain plot evaluated the steel modulus of elasticity. Based on the slope of the vertical displacement read from the LVDT versus load line, the steel modulus of elasticity was indirectly obtained as well. Any differences in the moduli of elasticity would signal stiffness discontinuities in the test setup, problems with alignments, or problematic readings from the strain gauge. The steel mockup specimen was always tested before and after each testing day. No changes in steel mockup specimen readings signaled no changes in the test setup alignment, nor any problems with the entire test apparatus including all electronic components. This simple test provided a surety of day-to-day correct reading continuity.

### *4.2.3. Specimen Details*

Each of the seven specimen groups contained 10 replicates. Every glass specimen was fully tempered. Tempering readings were provided by the manufacturer for all monolithic glass specimens. The same tempering levels and tempering variation are expected for the

laminated glass specimens. All glass sheets had a polished perimeter edge finish to eliminate any perimeter edge breakage when hole edge breakage was desired.

The dimensions of glass specimens were carefully chosen to eliminate any undesirable side effects related to the geometry of a glass specimen. The main restriction driving the specimen geometry was the standard size hole in the center of the glass specimens and the stress concentration around these holes. The width of a glass specimen must be sufficient enough to allow the stress to concentrate near the edge of a hole but remain invariable near the perimeter edges. For this study, the glass manufacturer was required to provide a standard size hole suitable for the typical fitting. The fitting manufacturer specifies the hole diameter of $d_h = 1.417\ inches$. Based on this assumed hole diameter, it was decided that at least twice this distance must be provided on both sided of the hole. This decision dictated the minimum glass specimen width of $7.1\ inches$. To provide some leeway, $8\ inch$ wide glass plates were selected. The same minimum $2d_h$ distance was used to determine the length of the constant moment region. Therefore, the distance between the loading edges was $8\ inches$ as well, which resulted in a $8\ x\ 8\ inch$ square constant moment region. The distance between the loading and bearing edges also had to be sufficient enough to allow the plate bending fracture to control the failure. Ultimate shear stresses must be lower than the ultimate bending stresses, and the shear force must travel from the loading edge to the bearing edge without any excessive values. The $3\ inch$ distance was determined as a suitable moment arm for four-point-bending testing. This adds up to the minimum specimen length of $14\ inches$. An extra $1\ inch$ was provided as overhang beyond the supporting edge. Therefore, the final glass specimen dimensions were 16 x 8 $x$ $0.5\ inches$ nominal. The dimensions of each specimen were

measured with a ruler and a digital caliper. The thickness $t$ was measured with the digital caliper at three points as depicted in Figure 25.

**Figure 25: Location of Thickness Measurements.**

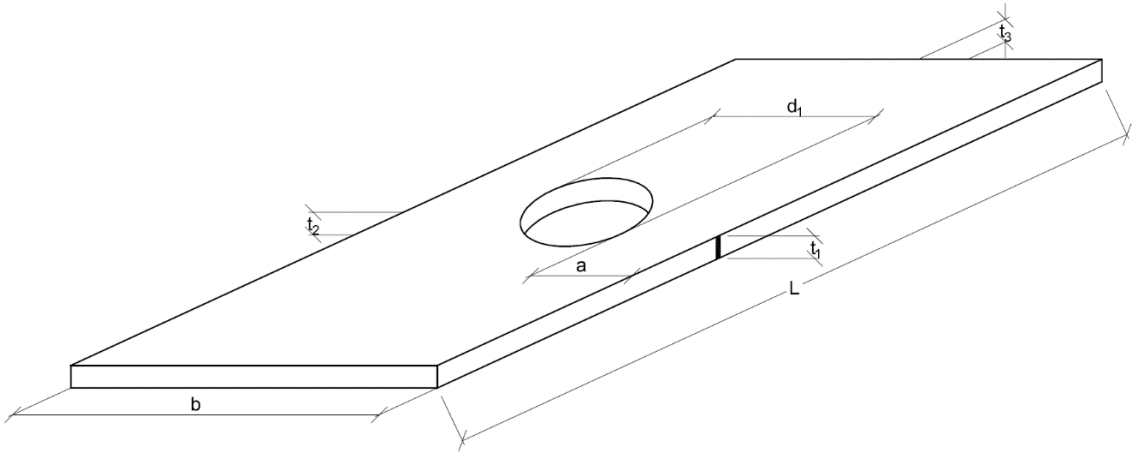


The average thickness across the middle of a specimen (i.e., between thicknesses $t_1$ and $t_2$) is reported in Table 7 through Table 13. The diameter $d_h$ of each hole was measured with the digital caliper in the transverse direction. Width $b$ of each specimen was measured in the middle section using the ruler with a resolution of $1/64\ inches$. For the laminated glass specimens, width $b$ and hole diameter $d_h$ were measured for both glass laminates. Typically, widths $b$ and hole diameters $d_h$ had different random values for the bottom and top glass laminates. Due to manufacturing concerns, the bottom hole diameters $d_{BOTTOM}$ were always oversized compared with the top diameters $d_{TOP}$ so that the holes do not overlap and ensure enough space for the fitting. All specimens were oriented in the test setup so that the greater hole was always in tension. The bottom hole diameter $d_{BOTTOM}$ was used for stress calculations. Table 7 through Table 13 summarize the measured actual dimensions of each specimen.

**Table 7: Monolithic Glass Dimensions – 4pt. Bending – No Hole.**

| Monolithic Glass - 4pt Bending - No Hole | | |
|---|---|---|
| Specimen # | t (in) | b (in) |
| 4N1 | 0.487 | 8.094 |
| 4N2 | 0.486 | 8.000 |
| 4N3 | 0.486 | 8.000 |
| 4N4 | 0.485 | 8.063 |
| 4N5 | 0.485 | 8.000 |
| 4N6 | 0.486 | 7.969 |
| 4N7 | 0.485 | 8.000 |
| 4N8 | 0.486 | 8.063 |
| 4N9 | 0.487 | 8.031 |
| 4N10 | 0.485 | 8.016 |
| Mean | 0.486 | 8.023 |
| St. Dev. | 0.001 | 0.036 |
| COV | 0.1% | 0.5% |

**Table 8: Monolithic Glass Dimensions – 4pt. Bending – With Hole.**

| Monolithic Glass - 4pt Bending - with Hole | | | |
|---|---|---|---|
| Specimen # | t (in) | b (in) | $d_h$ (in) |
| 4H1 | 0.487 | 8.063 | 1.432 |
| 4H2 | 0.494 | 8.000 | 1.432 |
| 4H3 | 0.495 | 8.016 | 1.433 |
| 4H4 | 0.495 | 8.016 | 1.433 |
| 4H5 | 0.494 | 8.000 | 1.433 |
| 4H6 | 0.498 | 8.016 | 1.430 |
| 4H7 | 0.486 | 8.016 | 1.434 |
| 4H8 | 0.495 | 8.016 | 1.430 |
| 4H9G | 0.486 | 7.969 | 1.433 |
| 4H10G | 0.485 | 8.047 | 1.428 |
| Mean | 0.491 | 8.016 | 1.432 |
| St. Dev. | 0.005 | 0.024 | 0.002 |
| COV | 0.9% | 0.3% | 0.1% |

**Table 9: Monolithic Glass Dimensions – 3pt. Bending – With Hole.**

| Monolithic Glass - 3pt Bending - with Hole | | | |
|---|---|---|---|
| Specimen # | t (in) | b (in) | $d_h$ (in) |
| 3H1 | 0.496 | 7.984 | 1.432 |
| 3H2 | 0.486 | 8.016 | 1.433 |
| 3H3 | 0.482 | 8.000 | 1.423 |
| 3H4 | 0.486 | 8.078 | 1.432 |
| 3H5 | 0.486 | 8.031 | 1.429 |
| 3H6 | 0.497 | 7.984 | 1.434 |
| 3H7 | 0.496 | 7.984 | 1.438 |
| 3H8 | 0.487 | 8.047 | 1.438 |
| 3H9G | 0.493 | 8.031 | 1.433 |
| 3H10G | 0.497 | 7.969 | 1.431 |
| Mean | 0.490 | 8.013 | 1.432 |
| St. Dev. | 0.005 | 0.033 | 0.004 |
| COV | 1.1% | 0.4% | 0.3% |

**Table 10: Monolithic Glass Dimensions – 4pt. Bending – Chamfered Hole Edges.**

| Monolithic - 4pt Bending - with Hole - Chamfered Hole Edge | | | |
|---|---|---|---|
| Specimen # | t (in) | b (in) | $d_h$ (in) |
| 4HP1 | 0.486 | 8.016 | 1.440 |
| 4HP2 | 0.486 | 8.000 | 1.432 |
| 4HP3 | 0.486 | 8.031 | 1.432 |
| 4HP4 | 0.485 | 8.000 | 1.444 |
| 4HP5 | 0.486 | 8.000 | 1.444 |
| 4HP6 | 0.486 | 8.000 | 1.443 |
| 4HP7 | 0.486 | 8.016 | 1.442 |
| 4HP8 | 0.486 | 8.000 | 1.443 |
| 4HP9 | 0.486 | 8.000 | 1.443 |
| 4HP10 | 0.486 | 8.016 | 1.438 |
| Mean | 0.486 | 8.008 | 1.440 |
| St. Dev. | 0.000 | 0.010 | 0.005 |
| COV | 0.1% | 0.1% | 0.3% |

**Table 11: Laminated Glass Dimensions – 4pt. Bending – No Hole.**

| Laminated Glass - 4pt Bending - No Hole | | | | | |
|---|---|---|---|---|---|
| Specimen # | $t_{BOTTOM}$ (in) | $t_{TOP}$ (in) | $t_{INTERLAYER}$ (in) | $b_{BOTTOM}$ (in) | $b_{TOP}$ (in) |
| | Measured | Measured | Assumed | | |
| 4NL1M | 0.223 | 0.227 | 0.060 | 8.063 | 8.063 |
| 4NL2M | 0.219 | 0.226 | 0.060 | 8.016 | 8.016 |
| 4NL3M | 0.221 | 0.227 | 0.060 | 7.984 | 8.047 |
| 4NL4 | 0.227 | 0.226 | 0.060 | 8.000 | 8.000 |
| 4NL5 | 0.221 | 0.217 | 0.060 | 8.031 | 8.031 |
| 4NL6 | 0.225 | 0.225 | 0.060 | 8.047 | 8.000 |
| 4NL7 | 0.227 | 0.227 | 0.060 | 8.016 | 8.016 |
| 4NL8 | 0.227 | 0.225 | 0.060 | 8.016 | 8.000 |
| 4NL9 | 0.225 | 0.225 | 0.060 | 8.016 | 8.016 |
| 4NL10G | 0.226 | 0.225 | 0.060 | 7.984 | 8.000 |
| Mean | 0.224 | 0.225 | 0.060 | 8.017 | 8.019 |
| St. Dev. | 0.003 | 0.003 | 0.000 | 0.024 | 0.021 |
| COV | 1.3% | 1.2% | 0.0% | 0.3% | 0.3% |

**Table 12: Laminated Glass Dimensions – 4pt. Bending – With Hole.**

| Laminated Glass - 4pt Bending - with Hole | | | | | | | |
|---|---|---|---|---|---|---|---|
| Specimen # | $t_{BOTTOM}$ (in) | $t_{TOP}$ (in) | $t_{INTERLAYER}$ (in) | $b_{BOTTOM}$ (in) | $b_{TOP}$ (in) | $d_{BOTTOM}$ (in) | $d_{TOP}$ (in) |
| | Measured | Measured | Assumed | | | | |
| 4HL1 | 0.222 | 0.225 | 0.060 | 7.938 | 7.984 | 1.660 | 1.507 |
| 4HL2 | 0.225 | 0.225 | 0.060 | 7.969 | 7.969 | 1.659 | 1.510 |
| 4HL3 | 0.222 | 0.225 | 0.060 | 8.047 | 8.063 | 1.622 | 1.432 |
| 4HL4 | 0.222 | 0.223 | 0.060 | 8.016 | 8.031 | 1.618 | 1.438 |
| 4HL5 | 0.221 | 0.222 | 0.060 | 8.016 | 8.000 | 1.613 | 1.424 |
| 4HL6 | 0.222 | 0.223 | 0.060 | 8.000 | 8.000 | 1.621 | 1.434 |
| 4HL7 | 0.223 | 0.224 | 0.060 | 7.969 | 7.984 | 1.655 | 1.512 |
| 4HL8 | 0.224 | 0.221 | 0.060 | 8.063 | 8.047 | 1.618 | 1.438 |
| 4HL9G | 0.225 | 0.224 | 0.060 | 7.984 | 7.969 | 1.660 | 1.508 |
| 4HL10G | 0.224 | 0.224 | 0.060 | 7.953 | 7.938 | 1.654 | 1.510 |
| Mean | 0.223 | 0.223 | 0.060 | 7.995 | 7.998 | 1.638 | 1.471 |
| St. Dev. | 0.001 | 0.001 | 0.000 | 0.038 | 0.037 | 0.020 | 0.038 |
| COV | 0.6% | 0.6% | 0.0% | 0.5% | 0.5% | 1.2% | 2.6% |

**Table 13: Laminated Glass Dimension – 3pt. Bending – With Hole.**

| Laminated Glass - 3pt Bending - with Hole | | | | | | | |
|---|---|---|---|---|---|---|---|
| Specimen # | $t_{BOTTOM}$ (in) | $t_{TOP}$ (in) | $t_{INTERLAYER}$ (in) | $b_{BOTTOM}$ (in) | $b_{TOP}$ (in) | $d_{BOTTOM}$ (in) | $d_{TOP}$ (in) |
| | Measured | Measured | Assumed | | | | |
| 3HL1 | 0.224 | 0.222 | 0.060 | 7.953 | 7.953 | 1.654 | 1.433 |
| 3HL2 | 0.223 | 0.227 | 0.060 | 7.953 | 7.984 | 1.655 | 1.513 |
| 3HL3 | 0.225 | 0.225 | 0.060 | 7.969 | 7.984 | 1.658 | 1.508 |
| 3HL4 | 0.221 | 0.225 | 0.060 | 7.953 | 8.063 | 1.659 | 1.441 |
| 3HL5 | 0.222 | 0.223 | 0.060 | 7.953 | 7.984 | 1.661 | 1.511 |
| 3HL6 | 0.222 | 0.224 | 0.060 | 7.984 | 7.969 | 1.654 | 1.512 |
| 3HL7 | 0.223 | 0.224 | 0.060 | 7.953 | 7.953 | 1.654 | 1.508 |
| 3HL8 | 0.225 | 0.219 | 0.060 | 7.984 | 8.031 | 1.607 | 1.426 |
| 3HL9G | 0.224 | 0.224 | 0.060 | 7.969 | 7.953 | 1.654 | 1.504 |
| 3HL10G | 0.218 | 0.222 | 0.060 | 7.953 | 7.984 | 1.654 | 1.511 |
| Mean | 0.223 | 0.223 | 0.060 | 7.963 | 7.986 | 1.651 | 1.487 |
| St. Dev. | 0.002 | 0.002 | 0.000 | 0.013 | 0.034 | 0.015 | 0.035 |
| COV | 0.9% | 0.9% | 0.0% | 0.2% | 0.4% | 0.9% | 2.4% |

One of the obstacles during the testing of both monolithic and laminated glass specimens utilizing the three-point-bending test setup was the amount of torque applied to the fitting to clamp the glass specimens. The glass fitting manufacturer recommends tightening the fittings up to the torque of $15\ lbf - ft$. With the wrench key provided by the manufacturer, it was impossible to achieve this torque or even measure the actual applied torque. As a result, an alternative procedure was developed. For each specimen, the fitting was finger-tightened to the maximum possible level, and utilizing a pair of groove pliers, an extra 1/10 turn was made. This created a constant level of clamp torque for each specimen that was tested.

## 4.3. Data Results

### *4.3.1. Pictures and Observations during Testing*

Each monolithic glass specimen behaved like a linear elastic material during testing, and was loaded to its ultimate failure. These breakage points occurred suddenly, catastrophically, and without any warning. The glass specimens broke into many small pieces that were catapulted in every direction. Surprisingly, the pieces were cast in an outward horizontal direction perpendicular to the test setup bearing edges. The strength with which these shards exploded was enormous, which indicated the high amounts of strain energy that monolithic glass can absorb. Figure 26 shows a typical load versus displacement plot for a single monolithic four-point bending with hole specimen.

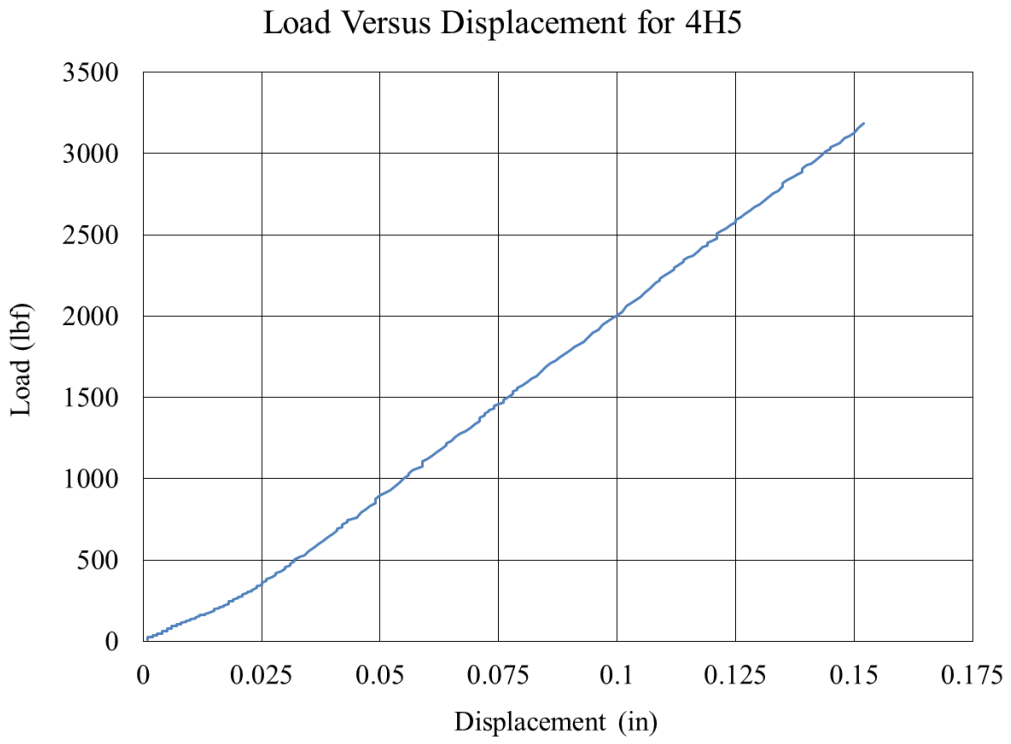


**Figure 26: Typical Load Versus Displacement for Monolithic Glass Specimens.**

The laminated glass specimens evinced linear behavior as well. This linear behavior was expected because the loading rate was slow enough to mimic steady loading conditions; however, at the same time, it was fast enough to prevent any relaxation and creep in the interlayer. Similar to the monolithic glass specimens, the failure of each laminated specimen occurred suddenly and without any warning as well. The advantage of laminated glass was that single pieces remained stuck to the interlayer, which is exactly the desirable safety feature that laminated glass possesses. Both glass laminates broke instantaneously for all specimen types except three specimens in the laminated glass – 4pt. Bending – No Hole set. Those three specimens broke laminate by laminate, indicating that the stresses were redistributed to the top laminate when the bottom laminate broke first. Figure 27 shows the typical breakage pattern of a four-point bending with hole specimen. Figure 28 plots a representative load versus displacement line for the same specimen.


**Figure 27: Typical Breakage of Laminated Glass.**

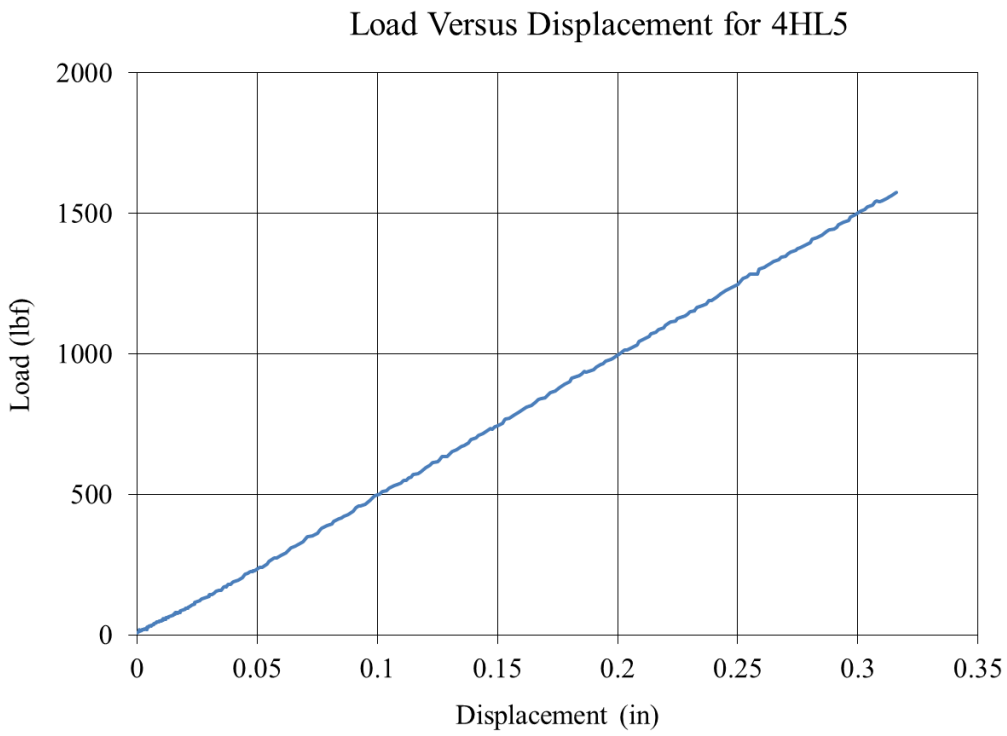


**Figure 28: Typical Load Versus Displacement Plot for Laminated Glass Specimens.**

### *4.3.2. ASTM E1300 Method for Effective Thickness of Laminated Glass*

The ASTM E1300 Standard [26] provides a formula for calculating the effective thickness of laminated glass. The purpose of this equation is to give engineers a tool that simplifies the design procedure by omitting the composite action of glass laminates. Instead, the formula treats the laminated glass as a monolithic material with a certain thickness that represents the laminated glass behavior as if it acted as a composite. There are two equations for effective thickness presented in the ASTM E1300 Standard. First, Equation (11) provides computations for the effective thickness of laminated glass used for deflection calculations. Equation (11) is

$$h_{ef;w} = \sqrt[3]{h_1^3 + h_2^3 + 12\Gamma I_s}. \tag{11}$$

Equation (11) is employed in Equations (12) and (13) to give the effective thickness used in stress calculations:

$$h_{1;ef;\sigma} = \sqrt{\frac{h_{ef;w}^3}{h_1 + 2\Gamma h_{s;2}}} \tag{12}$$

and

$$h_{2;ef;\sigma} = \sqrt{\frac{h_{ef;w}^3}{h_2 + 2\Gamma h_{s;1}}}, \tag{13}$$

where

$$\Gamma = \frac{1}{1 + 9.6\frac{EI_s h_v}{Gh_s^2 a^2}}, \tag{14}$$

with

$$I_s = h_1 h_{s;2}^2 + h_2 h_{s;1}^2 , \tag{15}$$

$$h_{s;1} = \frac{h_s h_1}{h_1 + h_2}, \tag{16}$$

$$h_{s;2} = \frac{h_s h_2}{h_1 + h_2}, \tag{17}$$

$$h_s = 0.5(h_1 + h_2) + h_v. \tag{18}$$

Values in Equations (12) through (18) are as follows

$h_v$ is the thickness of the PVB interlayer,

$h_1$ is the thickness of the top glass laminate,

$h_2$ is the thickness of the bottom glass laminate,

$E$ is the modulus of elasticity of glass,

$a$ is the smallest in-plane dimension of bending of laminate plate,

$G$ is the shear modulus of the PVB interlayer.

In the case of laminated glass specimens used in this research project, the thicknesses of the top and bottom glass laminates were equal $h_1 = h_2 = h$. Therefore, Equations (11) and (12) can be simplified to

$$h_{ef;w} = \sqrt[3]{2h^3 + 12\Gamma I_s}, \tag{19}$$

and

$$h_{ef;\sigma} = \sqrt{\frac{h_{ef;w}^3}{h + 2\Gamma h_s}}, \tag{20}$$

where

$$h_s = \frac{h + h_v}{2}, \tag{21}$$

$$I_s = \frac{h(h + h_v)^2}{2}, \tag{22}$$

and

$$\Gamma = \frac{1}{1 + 4.8\frac{E}{G}\frac{hh_v}{a^2}}. \tag{23}$$

The effect of the slight variances in thickness of each glass laminate is accounted for in this calculation, and the difference of effective thicknesses is insignificant. Consequently, the average glass laminate thickness $h = 0.225\ inches$, the assumed interlayer thickness $h_v = 0.06\ inches$, the shear modulus of $G = 242\ psi$, and the bending span $a = 14\ inches$ are used in calculating the effective thickness of laminated glass specimens. ASTM E1300 is meant for rectangular glass sheets that can be supported along their one, two, three, or four edges and subjected to uniformly distributed loads. The actual reading of ASTM E1300 specifies that $a$ is the "smallest in-plane dimension" of a laminate, which is the specimen width of 8 $inches$ in this specific study. However, according to Mr. Knowles of Stutzki Engineering, Inc., industry standard practice is to set variable $a$ to a value not less than the span for bending, so in this case $a = 14\ inches$ is used [31].

For all laminated glass stress calculations, the effective thickness of laminated glass is $h_{ef;\sigma} = 0.351\ inches.$

### *4.3.3. Stress Concentration from Strain Gauges*

#### 4.3.3.1. Stress Concentration Factor Based on Strain

Two specimens of each specimen type with a hole contained six strain gauges placed on the AB line depicted in Figure 29. Figure 30 shows the actual view of the applied strain gauges. The purpose of these strain gauges was to trace the stress flow around the hole and verify the stress concentration factor calculated using the Abaqus model and classical theories. Strain gauges, as their name suggests, measure the difference in strain. This strain can be converted to stress using Young's modulus of elasticity. The loading conditions used in this research project create the uniaxial bending of a plate. The expected stress flow direction of the uniaxial bending is parallel to the longitudinal edge and perpendicular to the bending moment axis. The four-point-bending test setup also creates a constant moment region between the loading points. Even though the resultant moment is constant, the hole creates an intrusion that the stress has to bypass, and therefore, the moment gets redistributed around the hole. Figure 29 shows the stress flow lines circumventing the hole intrusion and the stress line concentration in the very narrow part of the plate. This moment redistribution is

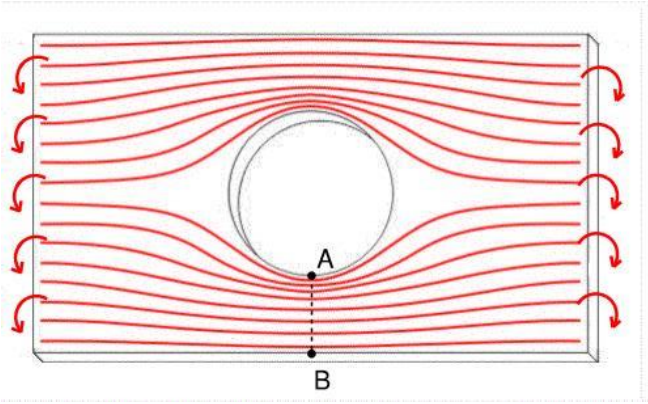


**Figure 29: Stress Lines of Uniaxial Bending.**

accompanied by shear stresses. The shear occurs in 45 degree directions since this is the area where moment redistribution takes place. This is visually characterized as the area where stress flow lines change their spacing. Because of symmetry, the stress flow lines are parallel to the longitudinal edge in the narrowest part of the glass. No moment redistribution nor shear stresses occur. Strain gauges were placed in this narrow part between point A and B to measure the expected maximum strain (see Figure 30). Figure 31 shows a typical applied load versus strain line of the four-point bending of

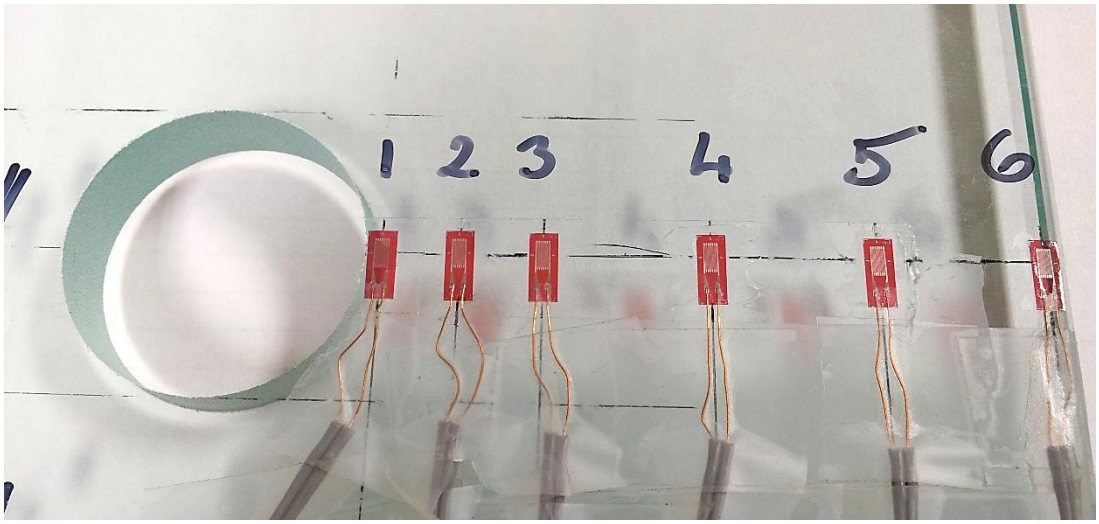


**Figure 30: Strain Gauges Applied to Specimen.**

specimen 4H10G (monolithic glass specimen with a hole). It is very clear that strain increases with the applied load linearly. The same linear relationship between the applied load and strain was observed for both monolithic and laminated specimens. This demonstrates that both monolithic and laminated specimens behave with perfect linear-elasticity at testing room temperature and a loading speed of 10,000 psi/min. This also means that the stress concentration factor from the strain gauges can be calculated at any

load since the readings from all strain gauges of one specimen are relative to each other. A set of strain gauge readings at any load is only a superposition of other sets at any load.

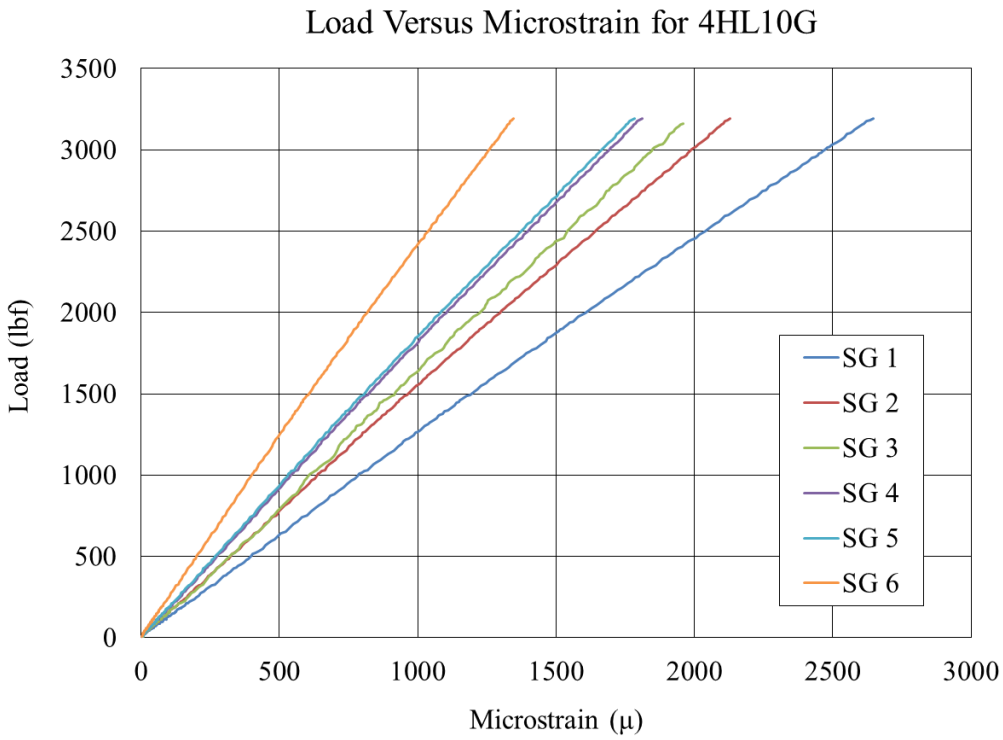


**Figure 31: Typical Load Versus Strain Plot for Monolithic and Laminated Glass Specimens.**

Knowing this linear relationship between the applied load and strain, a random common load was assigned to each specimen type at which the stress concentration factor was calculated. For monolithic four-point bending, the load at which the stress concentration factor was calculated was $2400lbf$. For monolithic three-point-bending specimens, it was $1200lbf$. The strain gauge stress concentration factor for monolithic glass specimens with a chamfered hole edge was calculated at the common load of $2400lbf$. For laminated glass specimens subjected to four-point bending, the common load was

$1800lbf$. And for laminated specimens subjected to three-point bending, it was $700lbf$. These loads are close to the breaking point of each specimen type. However, the same stress concentration factor would have been obtained at any increased or decreased load. Figure 32 through Figure 36 show a plot of strain versus distance from the edge of a hole. Strain gauges applied to two specimens in each specimen group allowed for the strain to be measured at the aforementioned common loads. The four-point-bending monolithic glass specimens with a chamfered hole edge had three specimens with six strain gauges on each.

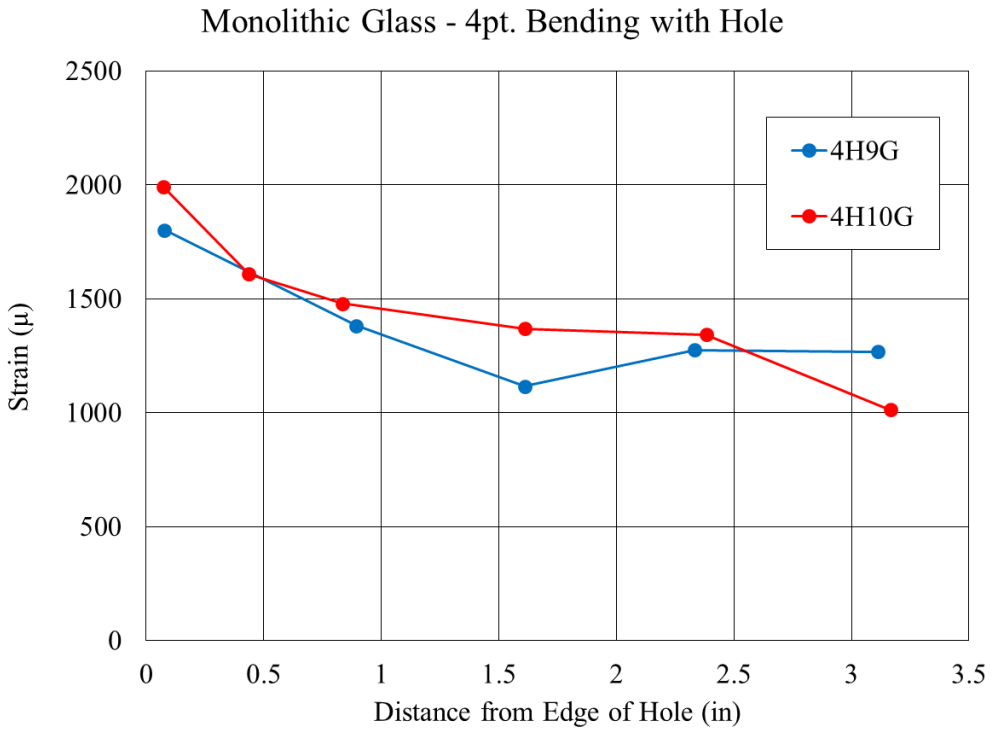


**Figure 32: Monolithic Glass Specimens with Hole – 4pt. Bending.**

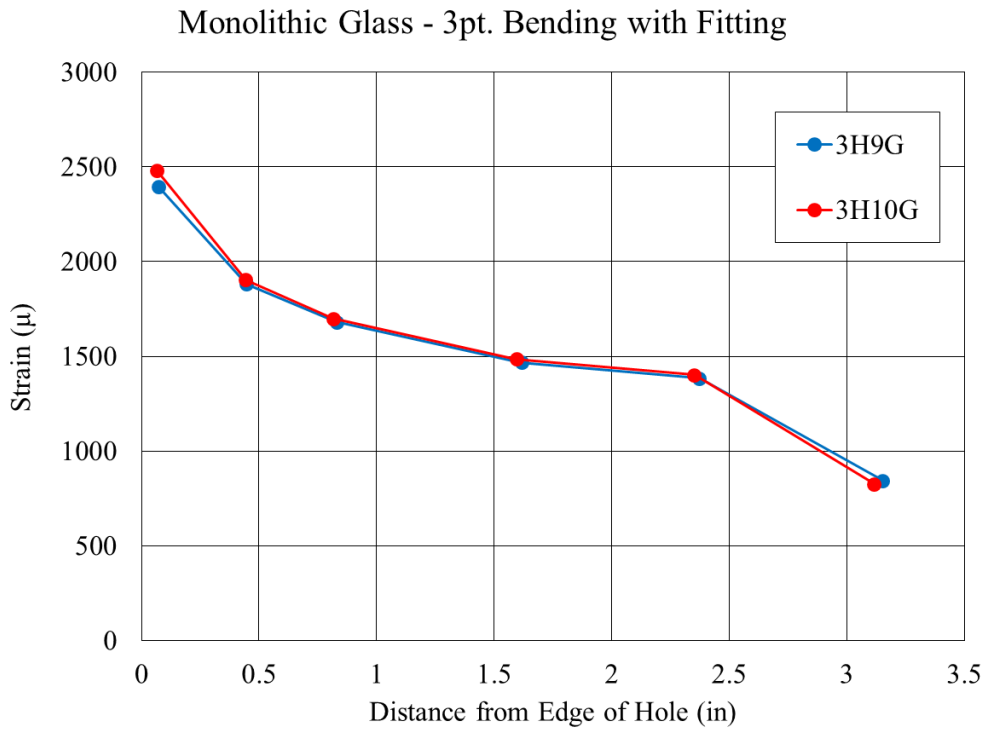


**Figure 33: Monolithic Glass Specimens with Hole – 3pt. Bending.**

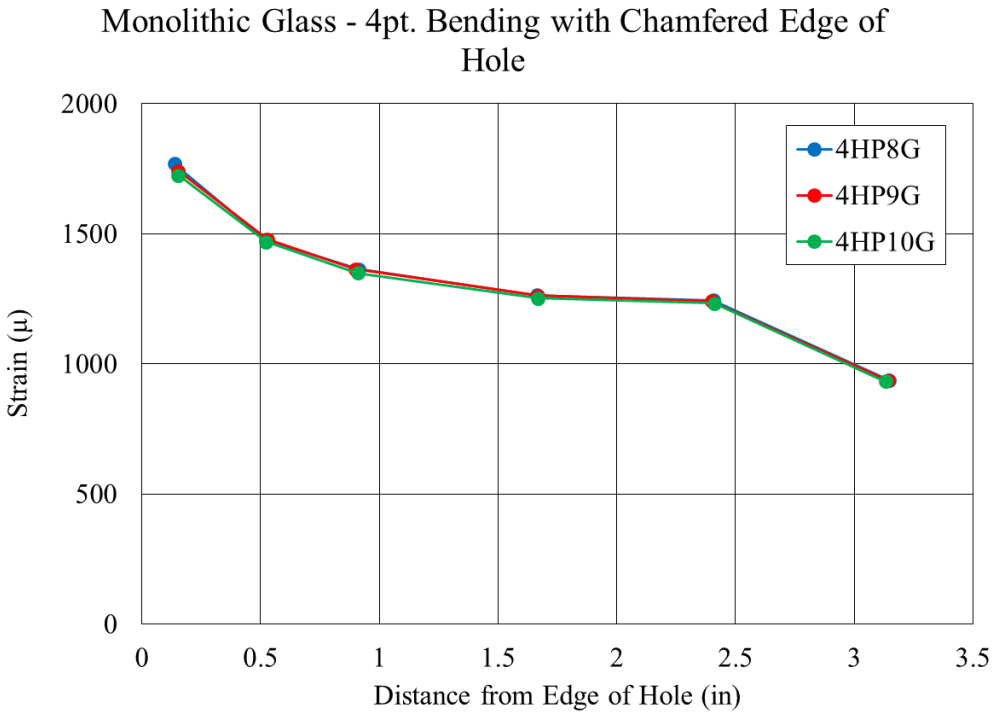


**Figure 34: Monolithic Glass Specimens with Chamfered Edge of Hole – 4pt. Bending.**

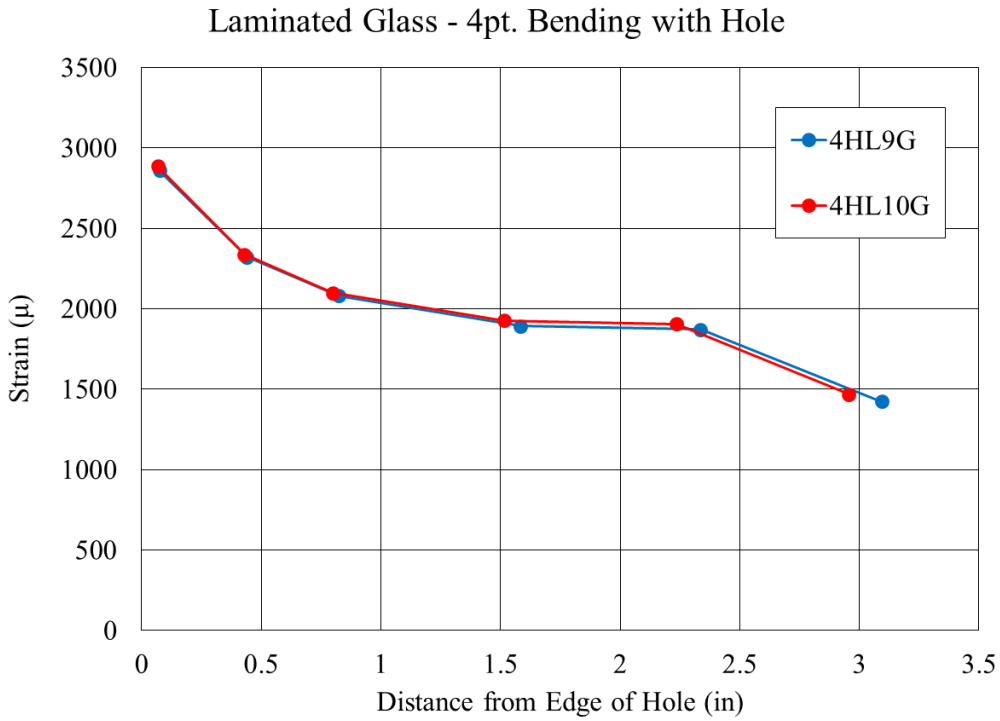


**Figure 35: Laminated Glass Specimens with Hole – 4pt. Bending.**

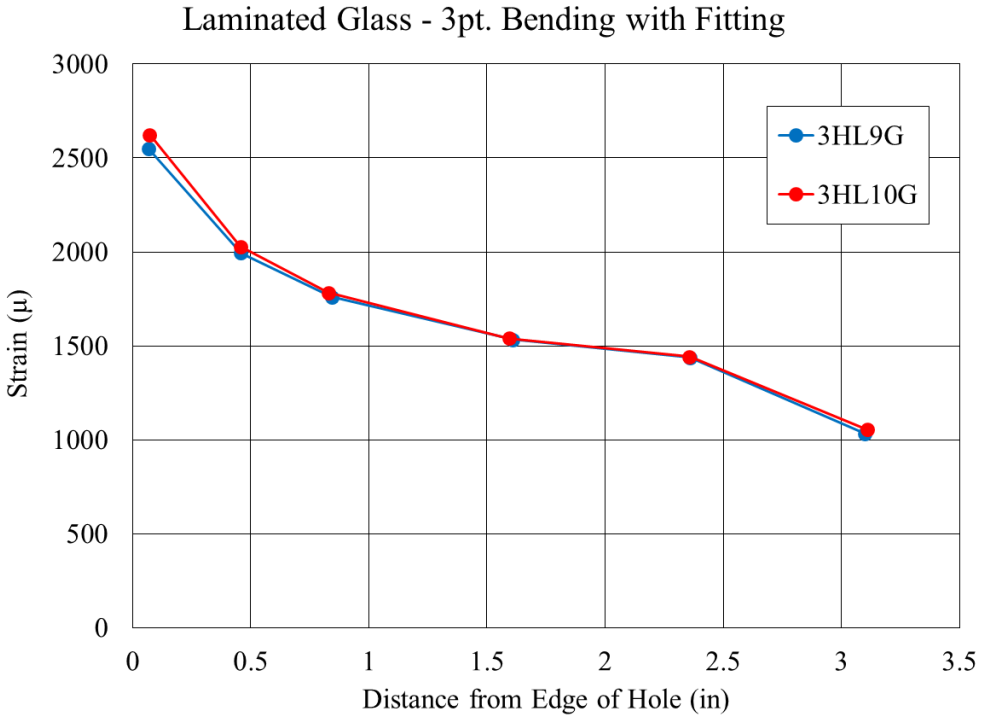


**Figure 36: Laminated Glass Specimens with Hole – 3pt. Bending.**

The equation for the net section stress concentration factor can be rewritten as $K_{net} = \frac{\sigma_{peak}}{\sigma_{net}} = \frac{E.\epsilon_{peak}}{E.\epsilon_{net}} = \frac{\epsilon_{peak}}{\epsilon_{net}}$. This simplification eliminates any uncertainty in Young's modulus of elasticity. The net section stress concentration is calculated strictly from the strain gauges.

The readings from the strain gauges take the form of an isolated value. They provide an idea of what the strain is at certain points. The strain distribution between the strain gauge readings can only be assumed. However, the obtained strain readings in this research project follow the expected stress distribution, which signal a very strong correlation between the theory and the real test specimen. In order to calculate the stress concentration factor, the peak strain and net average strain must be known. Unfortunately, the peak strain is known only at a short distance from the edge of the hole, and the average strain is unknown. This challenge of discontinuity in strain readings was overcome through the utilization of a curve fit to the known strain points. To extrapolate between strain points, a fourth-order polynomial function was used. This function was chosen based on the fact that the solution of the differential equation for plates is of the same fourth order. The Excel trend-line function was used to generate the most fitting fourth-order polynomial function. This fourth-order polynomial function is defined as $\epsilon(x) = ax^4 + bx^3 + cx^2 + dx + C$ where $(x)$ is the variable distance from the edge of the hole. The peak strain is the maximum strain at the edge of the hole where $x = 0$; substituting $x = 0$ into the equation, the peak strain is $\epsilon_{peak} = C$. The average strain is then calculated using the integral of the strain function. The function average is calculated as

$$\epsilon_{net} = \frac{1}{q-p}\int_{p}^{q} ax^4 + bx^3 + cx^2 + dx + C$$
$$= \frac{1}{q-p}\left[\frac{a}{5}x^5 + \frac{b}{4}x^4 + \frac{c}{3}x^3 + \frac{d}{2}x^2 + Cx\right]_p^q. \quad (24)$$

Before final curves were fitted to the strain points, there were a few adjustments that had to be made. It is noticeable that the strain readings from the very perimeter strain gauge drop significantly below the values of the middle region with an almost constant strain. This repeating trend reveals that there must be an edge effect causing these strain readings to drop below the constant values. All specimens were finished with chamfered perimeter edges. This chamfer was as much as $0.070\ inches$ wide and thick, which was large enough to vary the edge stresses of the specimen. To allow for a reasonable curve fit, this last strain reading was eliminated from the data point series. This decision was based on the knowledge that both the classical and Abaqus theories predict a constant stress region at the very edge of a specimen with no significant stress drop as observed.

The strain readings from specimen 4H9G did not fit appropriately with the data from all other specimens' strain readings. This strain reading discrepancy was influenced by several circumstances. The first issue arose from the fact that this was the first specimen the strain gauges were applied to. Additionally, the strain reading from the third strain gauge was lower than the readings from the second and fourth strain gauges. Based on these strain readings, there should be a sinkhole in the stress flow, but that is impossible. Therefore, the reading from this strain gauge is not correct and has been eliminated from the set of points for the curve fit. The second issue was that there was not a strain gauge

applied between the first and second strain gauges. As a result, it was difficult to predict a smooth increase in strain close to the edge of the hole. Both of these issues must be kept in mind when assessing the stress concentration factor for specimen 4H9G.

Table 14 summarizes the thickness $t$, the net section stress concentration factor calculated from strain gauges $K_{netEXP}$, and the net section stress concentration factor calculated using Roark's formula $K_{netROARK}$ of each specimen. The plus sign indicates that the experimental stress concentration factor is less than the stress concentration factor calculated using Roark's formula. The minus sign stipulates that $K_{netEXP} > K_{netROARK}$.

**Table 14: Experimental Stress Concentration Factor Comparison.**

| Specimen # | t or $t_{eff}$ (in) | $K_{netEXP}$ | $K_{netROARK}$ | % Difference |
|---|---|---|---|---|
| 4H9G | 0.486 | 1.365 | 1.654 | 17.5% |
| 4H10G | 0.485 | 1.443 | 1.654 | 12.7% |
| 3H9G | 0.49275 | 1.589 | 1.654 | 3.9% |
| 3H10G | 0.4965 | 1.628 | 1.654 | 1.6% |
| 4HL9G | 0.351 | 1.475 | 1.537 | 5.5% |
| 4HL10G | 0.351 | 1.464 | 1.537 | 6.3% |
| 3HL9G | 0.351 | 1.610 | 1.537 | -3.1% |
| 3HL10G | 0.351 | 1.651 | 1.537 | -5.7% |
| 4HP8G | 0.4855 | 1.381 | 1.654 | 16.5% |
| 4HP9G | 0.486 | 1.360 | 1.654 | 17.8% |
| 4HP10G | 0.48625 | 1.357 | 1.654 | 18.0% |

When the net section stress concentration factors from the strain gauges were compared to those from Roark's reference, the strain gauges from all specimen types – except those of the three-point bending of laminated glass – predicted a lower stress concentration factor than the theory. This demonstrates a more uniform and less rapid stress increase

across the distance between the hole edge and side edge of a specimen. This prediction of the strain gauges is not fully understood. There is no clear explanation as to why the strain gauges predict a more uniform stress distribution than what the FE model and classical analytical model predict. The difference between the strain gauge net section stress concentration factors and Roark's formula stress concentration factor is within the range of $1.6 - 18.0\%$. Roark's formula was utilized to convert the experimental ultimate load to peak stresses in Section 4.3.4.

4.3.3.2. Stress Concentration Comparison Based on Stress

The same comparison of the stress concentration factors can be accomplished using stresses. The microstrain can be converted to stresses using Young's modulus of elasticity for glass, which is $E = 10400\ ksi$. This value is also in accordance with the modulus of elasticity obtained from the vertical deflection readings of the monolithic glass specimens with no holes. The advantage of comparing peak stresses is that Reissner's stress concentration factor, Roark's stress concentration factor, and the FE stress prediction can be compared with the actual converted stresses. A common load of $1000\ lbf$ was assigned to this comparison.

The corresponding moment to this load was calculated for three-point-bending and four-point-bending test setups. The gross section and net section module were calculated and used to divide the moment to get the average net section and gross section stresses:

$$S_{gross} = \frac{b.t^2}{6} \tag{25}$$

and

$$S_{net} = \frac{(b - d_h).\, t^2}{6}, \tag{26}$$

where

$b = glass\ plate\ width,$

$d_h = hole\ diameter,$

$t = glass\ plate\ thickness,$

and

$$\sigma_{gross} = \frac{M}{S_{gross}}, \tag{27}$$

$$\sigma_{net} = \frac{M}{S_{net}}. \tag{28}$$

Effective thickness was utilized in Equations (25) and (26) for laminated glass. Roark's Equation (9) and Reissner's Equation (7) were used to predict the peak stresses:

$$\sigma_{peak} = K_{gross}\, \sigma_{gross}\,, \tag{29}$$

$$\sigma_{peak} = K_{net}\, \sigma_{net}. \tag{30}$$

The four-point bending and three-point bending of monolithic glass specimens with a hole was simulated using the FE model. A comparison of these theories is displayed in Figure 37 through Figure 41. The effective thickness of laminated glass specimens is 0.351 *inches* as discussed in Section 4.3.2.

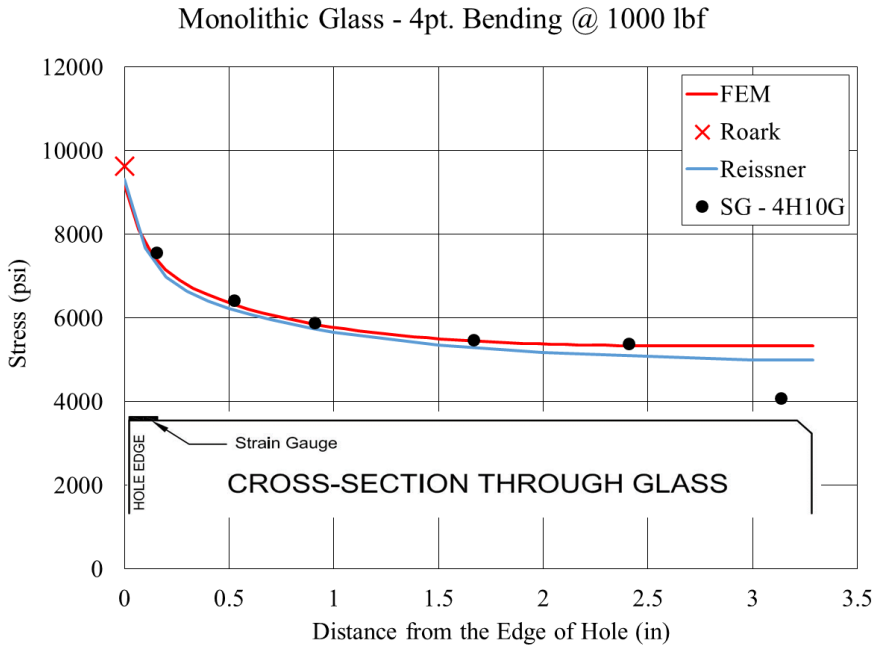


**Figure 37: Stress Concentration Comparison – Monolithic Glass Specimen – 4pt. Bending.**

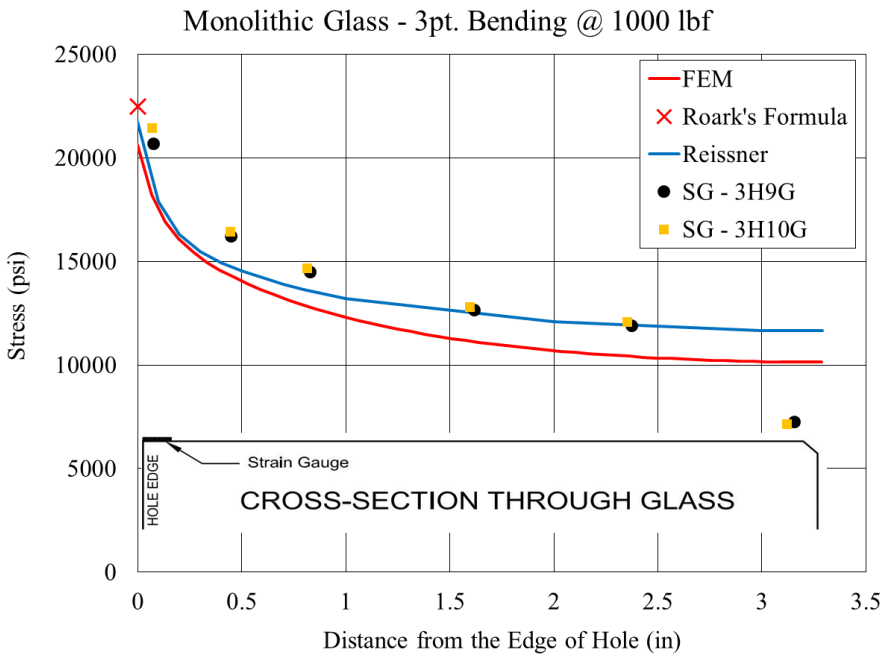


**Figure 38: Stress Concentration Comparison – Monolithic Glass Specimen – 3pt. Bending.**

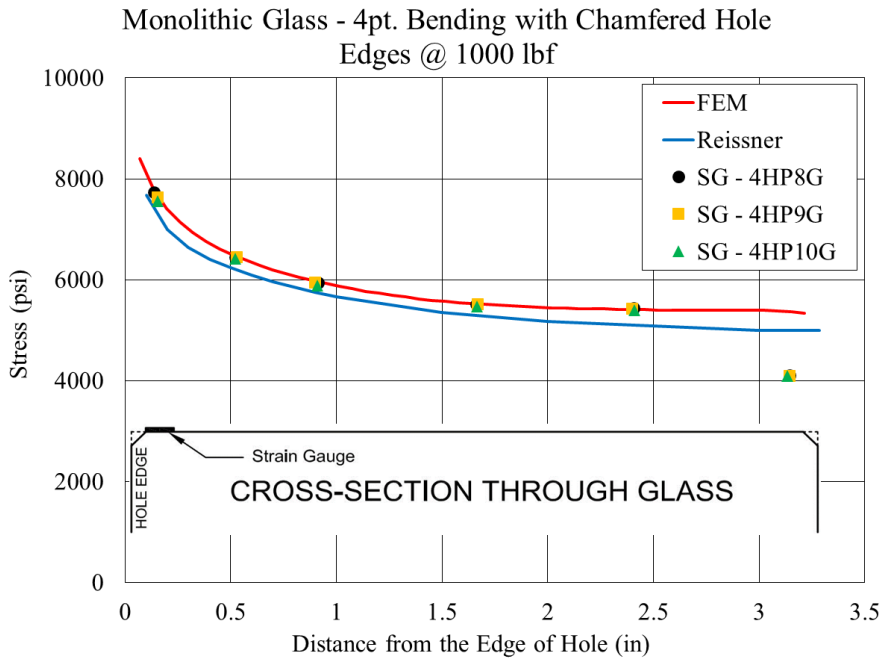


**Figure 39: Stress Concentration Comparison – Monolithic Glass Specimen with Chamfered Edge of Hole – 4pt. Bending.**

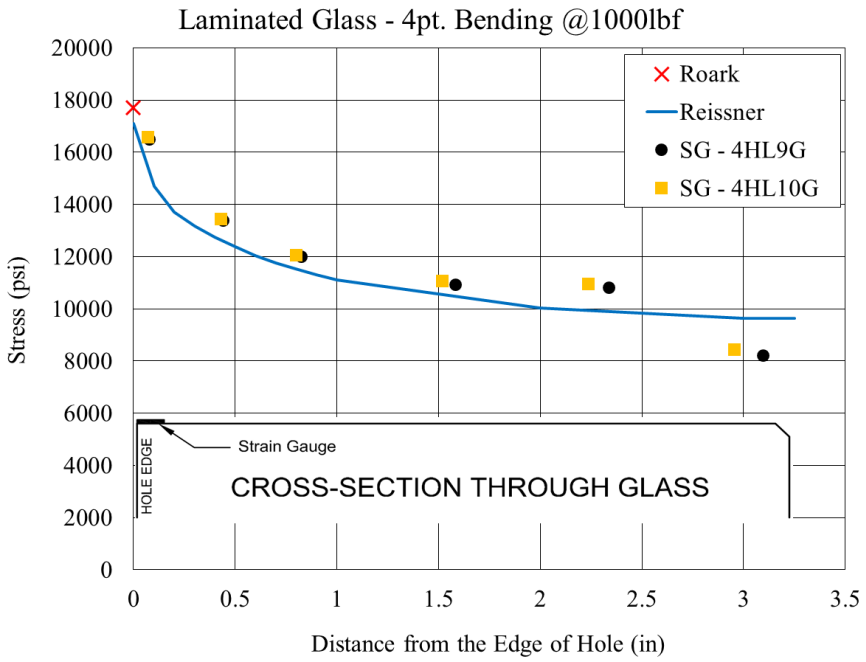


**Figure 40: Stress Concentration Comparison – Laminated Glass Specimen – 4pt. Bending.**

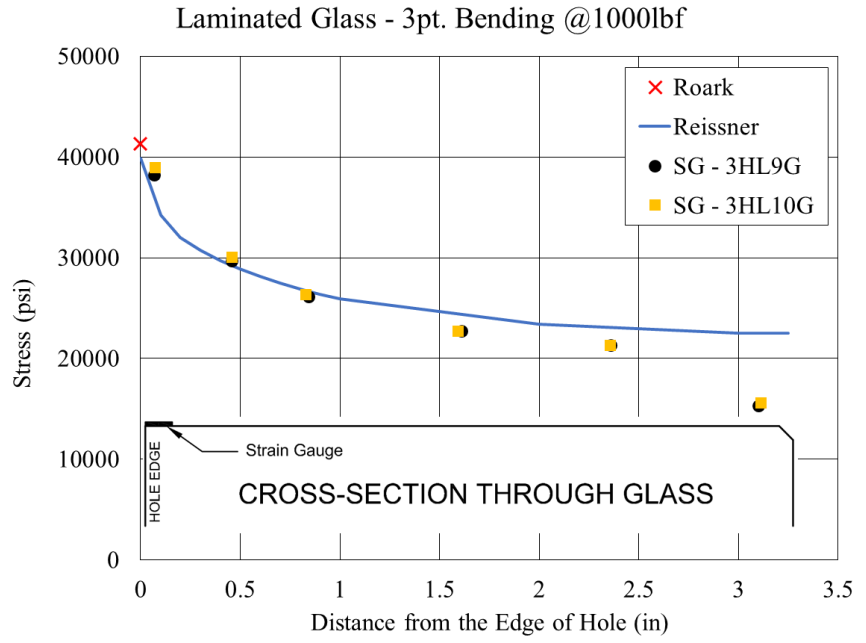


**Figure 41: Stress Concentration Comparison – Laminated Glass Specimen – 3pt. Bending.**

The strain gauge readings at the very edge of a specimen exhibited a much lower strain than the two adjacent strain gauges in the middle of the specimen. This phenomenon was caused by the edge effect of chamfered longitudinal edges. If this reading from the edge strain gauge was left out, the theoretically determined stresses and actual readings from the strain gauges matched.

### ***4.3.4.*** *Strength of Glass*

The ultimate force applied to each glass specimen created an ultimate moment. This ultimate force was converted to an ultimate moment using a simple formula: $(Moment\ arm)$ x $(Reaction)$. For four-point bending, the moment was $(1.5\ inches)$ x $(Ultimate\ Force)$, and for three-point bending the moment was $(3.5\ inches)$ x $(Ultimate\ Force)$, resulting in an ultimate moment with units of $lbf - inches$. The net section modulus of each glass specimen was determined from the formula

$$S_{net} = \frac{(b - d_h)(t)^2}{6}, \tag{31}$$

where $b$ is the width of a specimen, $d_h$ is the hole diameter, and $t$ is the specimen thickness for monolithic glass. The average effective thickness $t_{eff}$ was used in this formula for calculating the net section modulus of laminated glass. ASTM E1300 Equation (20) for effective thickness $t_{eff}$ [26] offsets any small differences between glass laminate thicknesses. The difference between accounting for each laminate's actual thickness and taking the average of all the glass laminates is within 1%. For practical

reasons, this difference is negligible. The average stress was found utilizing the equation $\sigma_{net} = \frac{M}{S_{net}}$. In order to ascertain the peak stress at the edge of a hole, this net average stress was multiplied by Roark's stress concentration factor. Roark's stress concentration factor was calculated using the average thickness $t$ or $t_{eff}$, the average width $b$, and the average hole diameter $d_h$. The stress concentration factor does not differ more than 1% if the actual dimensions were used in Equation (9). For practical purposes, the average stress concentration factor was utilized. The peak stress is $\sigma_{peak} = K_{net}\sigma_{net}$.

Table 15 through Table 21 summarize these calculations for each specimen. $K_{net}$ for monolithic glass based on $t_{avg} = 0.485\ inches$ is 1.654 and $K_{net}$ for laminated glass based on $t_{eff} = 0.351\ inches$ is 1.537.

**Table 15: Strength of Monolithic Glass – 4pt. Bending – No Hole.**

| **Monolithic Glass - 4pt Bending - No Hole** | | | | | |
|---|---|---|---|---|---|
| Specimen # | Load (lbf) | $M_{max}$ (lbf-in) | $S_{net}$ ($in^3$) | $\sigma_{net}$ (psi) | $\sigma_{peak}$ (psi) |
| 4N1 | 6862 | 10292 | 0.320 | 32170 | 32170 |
| 4N2 | 5600 | 8400 | 0.315 | 26670 | 26670 |
| 4N3 | 6629 | 9943 | 0.315 | 31570 | 31570 |
| 4N4 | 5882 | 8822 | 0.316 | 27880 | 27880 |
| 4N5 | 6133 | 9199 | 0.314 | 29300 | 29300 |
| 4N6 | 6593 | 9890 | 0.313 | 31560 | 31560 |
| 4N7 | 6055 | 9082 | 0.314 | 28930 | 28930 |
| 4N8 | 5558 | 8337 | 0.317 | 26290 | 26290 |
| 4N9 | 6292 | 9438 | 0.317 | 29730 | 29730 |
| 4N10 | 6393 | 9590 | 0.315 | 30490 | 30490 |
| Mean | 6199 | 9299 | 0.316 | 29460 | 29460 |
| St. Dev. | 415 | 622 | 0.002 | 1947 | 1947 |
| COV | 6.7% | 6.7% | 0.6% | 6.6% | 6.6% |

Since there are no holes in this set of specimens, the net average stress across a specimen equals the peak stress at which the specimen broke. The mean stress value represents the base strength of a monolithic fully tempered glass. This glass strength of $\sigma_{ult} = 29460\ psi$ is greater than expected. Common practice in the glass industry is to assume the ultimate strength of monolithic fully tempered glass to be $\sigma_{ult} = 24000\ psi$. ASTM E1300 specifies the allowable edge stress to be $\sigma_{allowable} = 10600\ psi$ [26]. This allowable stress is almost three times lower than the observed actual ultimate stress, providing a safety factor of 3.

**Table 16: Strength of Monolithic Glass – 4pt. Bending – With Hole.**

| Monolithic Glass - 4pt. Bending - with Hole | | | | | |
|---|---|---|---|---|---|
| Specimen # | Load (lbf) | $M_{max}$ (lbf-in) | $S_{net}$ ($in^3$) | $\sigma_{net}$ (psi) | $\sigma_{peak}$ (psi) |
| 4H1 | 3013 | 4519 | 0.262 | 17280 | 28580 |
| 4H2 | 3065 | 4597 | 0.267 | 17210 | 28460 |
| 4H3 | 3072 | 4607 | 0.269 | 17160 | 28380 |
| 4H4 | 2973 | 4460 | 0.269 | 16610 | 27470 |
| 4H5 | 3183 | 4775 | 0.267 | 17880 | 29570 |
| 4H6 | 3217 | 4826 | 0.272 | 17760 | 29380 |
| 4H7 | 3125 | 4687 | 0.259 | 18090 | 29920 |
| 4H8 | 3178 | 4766 | 0.269 | 17740 | 29340 |
| 4H9G | 2426 | 3639 | 0.257 | 14140 | 23390 |
| 4H10G | 3195 | 4792 | 0.259 | 18470 | 30540 |
| Mean | 3044 | 4567 | 0.265 | 17230 | 28500 |
| St. Dev. | 220 | 331 | 0.005 | 1147 | 1898 |
| COV | 7.2% | 7.2% | 1.8% | 6.7% | 6.7% |

The average ultimate strength of a glass specimen with a hole is $\sigma_{hole-ult} = 28500\ psi$. The presence of a water-jet drilled hole reduces the ultimate strength of fully tempered monolithic glass by 3.3%. The coefficient of variation ($COV$=6.7%) is very tight for monolithic glass specimens both with and without a hole. The AAMA document

specifies that the average coefficient of variation of fully tempered monolithic glass is 10% [24]. The results for fully tempered monolithic glass are well within this limit.

**Table 17: Strength of Monolithic Glass – 3pt. Bending – With Hole.**

| Monolithic Glass - 3pt Bending - with Fitting | | | | | |
|---|---|---|---|---|---|
| Specimen # | Load (lbf) | $M_{max}$ (lbf-in) | $S_{net}$ ($in^3$) | $\sigma_{net}$ (psi) | $\sigma_{peak}$ (psi) |
| 3H1 | 1217 | 4260 | 0.269 | 15860 | 26230 |
| 3H2 | 1026 | 3590 | 0.259 | 13880 | 22960 |
| 3H3 | 1014 | 3549 | 0.255 | 13940 | 23050 |
| 3H4 | 1062 | 3715 | 0.262 | 14190 | 23460 |
| 3H5 | 1036 | 3626 | 0.260 | 13940 | 23050 |
| 3H6 | 1101 | 3854 | 0.269 | 14320 | 23690 |
| 3H7 | 1078 | 3773 | 0.269 | 14040 | 23220 |
| 3H8 | 1095 | 3831 | 0.261 | 14700 | 24310 |
| 3H9G | 1365 | 4778 | 0.267 | 17890 | 29590 |
| 3H10G | 1331 | 4657 | 0.269 | 17340 | 28680 |
| Mean | 1132 | 3963 | 0.264 | 15010 | 24820 |
| St. Dev. | 121 | 422 | 0.005 | 1421 | 2351 |
| COV | 10.7% | 10.7% | 1.9% | 9.5% | 9.5% |

The average ultimate strength of a glass specimen with load applied via fitting is $\sigma_{fitting-ult} = 24820\ psi$. This loading condition and the presence of the fitting reduces the strength of a glass specimen with a hole by a further 12.9%. This also means that the load capacity of a point-supported glass with a standard swivel fitting is 84.2% of the full capacity of the glass sheet itself. In other words, the strength of a glass sheet is reduced by 15.8% due to the specific way it is supported in a structure. The coefficient of variation is also greater than monolithic glass with and without hole. This can be explained as a result of the contact uncertainty between the fitting and glass.

**Table 18: Strength of Monolithic Glass – 4pt. Bending – Chamfered Hole Edges.**

| Monolithic - 4pt. Bending - with Hole - Chamfered Hole Edge* | | | | | |
|---|---|---|---|---|---|
| Specimen # | Load (lbf) | $M_{max}$ (lbf-in) | $S_{net}$ ($in^3$) | $\sigma_{net}$ (psi) | $\sigma_{peak}$ (psi) |
| 4HP1 | 3874 | 5811 | 0.259 | 22420 | 30400 |
| 4HP2 | 3503 | 5255 | 0.259 | 20320 | 27560 |
| 4HP3 | 3345 | 5017 | 0.260 | 19330 | 26210 |
| 4HP4 | 3574 | 5361 | 0.257 | 20860 | 28280 |
| 4HP5 | 3881 | 5822 | 0.258 | 22600 | 30650 |
| 4HP6 | 3459 | 5189 | 0.258 | 20120 | 27280 |
| 4HP7 | 3438 | 5157 | 0.259 | 19930 | 27030 |
| 4HP8 | 3578 | 5366 | 0.258 | 20830 | 28250 |
| 4HP9 | 3795 | 5692 | 0.258 | 22050 | 29900 |
| 4HP10 | 3755 | 5633 | 0.259 | 21730 | 29470 |
| Mean | 3620 | 5430 | 0.258 | 21020 | 28500 |
| St. Dev. | 183 | 274 | 0.001 | 1069 | 1450 |
| COV | 5.0% | 5.0% | 0.3% | 5.1% | 5.1% |

**Calculated using net stress concentration factor $K_{net-chamfer} = 1.356$*

One of the breakthrough discoveries that came about while testing the monolithic glass is that if the hole edges are chamfered by as little as $0.07\ in$, the stress concentrations are significantly less than when the hole edge is not chamfered. The explanation of this phenomenon is that the chamfer shifts the breaking point where the glass rupture starts farther away from the edge of the hole as depicted in Figure 42. Varying the position of the breaking point decreases the peak stress value as shown in Figure 43. The rapid increase in stress is close to the edge of a hole. Consequently, shifting the critical breaking point as little as $0.07\ in$ farther away from the edge of a hole significantly lowers stresses at the same load.

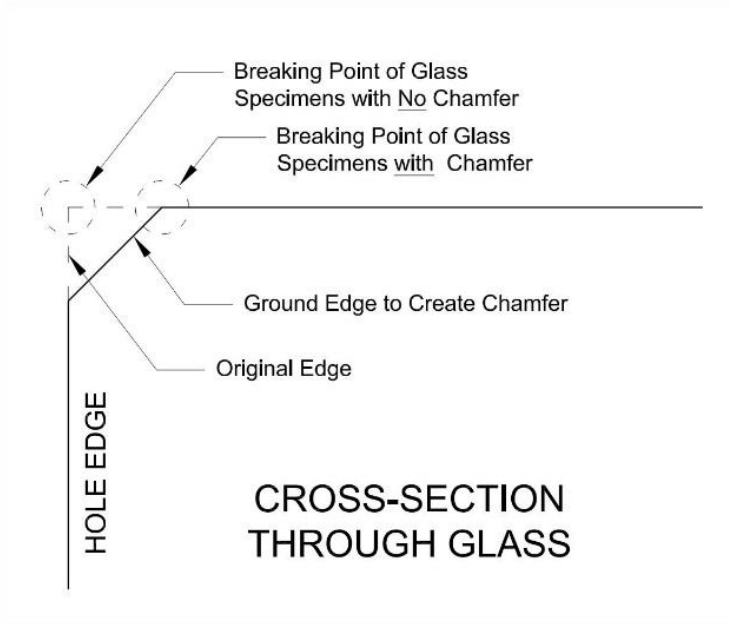


**Figure 42: Edge of Hole Detail.**

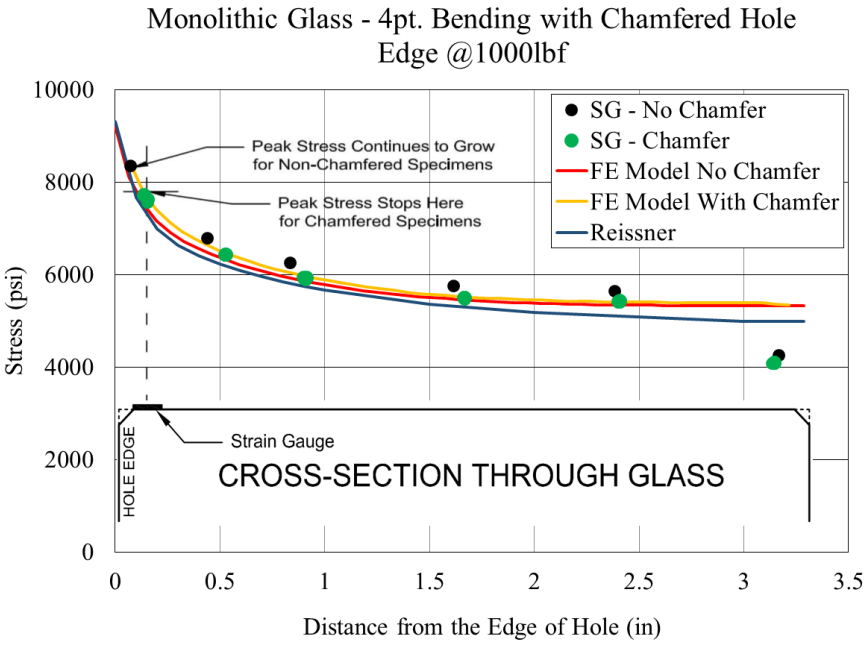


**Figure 43: Stress Concentration at Chamfered Hole.**

As shown in Figure 43, the first strain gauge was placed at the edge of the chamfer for specimens with chamfered holes, and Figure 30 shows that the first strain gauge was placed directly at the edge of the hole for specimens with non-chamfered holes. The strain gauge readings at the *breaking* load indicate that the strain at the breaking point was the same for all specimens with and without the chamfered edge of a hole subjected to four-point bending. Assuming a constant for Young's modulus of elasticity across all specimens, the breaking stress was the same for specimens with and without a chamfered hole edge. Therefore, the increased moment capacity of glass specimens with the chamfered hole edge can be attributed to reduced stress concentration. The derivation of the new stress concentration factor is found by assuming that both specimen types have the same material strength $\sigma_{ult}$ and comparing the ratio of this peak stress to the average stress on the net cross-section $\sigma_{chamfer-avg}$. The derivation is

$$\sigma_{hole-ult} = 28500\ psi\ , \tag{32}$$

$$\sigma_{chamfer-ult} = K_{net-chamfer}\sigma_{chamfer-avg}\ , \tag{33}$$

$$K_{net-chamfer} = \frac{\sigma_{hole-ult}}{\sigma_{chamfer-avg}}, \tag{34}$$

$$K_{net-chamfer} = \frac{28500}{21020} = 1.356. \tag{35}$$

This new stress concentration factor for chamfered edges $K_{net-chamfer} = 1.356$ predicts the stresses at the edge of a chamfered hole edge and is compared to $K_{net} = 1.654$ for specimens with no chamfer. The chamfer increases the capacity of a panel with a hole as much as $\left(1 - \frac{1.356}{1.654}\right)(100) = 18\%$. This is an important discovery for both designers and manufacturers alike because in choosing holes with chamfered edge finishes, they can get a higher capacity out of the same glass panel.

**Table 19: Strength of Laminated Glass – 4pt. Bending – No Hole.**

| Laminated Glass - 4pt. Bending - No Hole | | | | | |
|---|---|---|---|---|---|
| Specimen # | Load (lbf) | $M_{max}$ (lbf-in) | $t_{eff}$ (in) | $S_{net}$ ($in^3$) | $\sigma_{peak}$ (psi) |
| 4NL1M | 2897 | 4345 | 0.351 | 0.166 | 26250 |
| 4NL2M | 2788 | 4183 | 0.351 | 0.165 | 25410 |
| 4NL3M | 2064 | 3095 | 0.351 | 0.164 | 18880 |
| 4NL4 | 2896 | 4343 | 0.351 | 0.164 | 26440 |
| 4NL5 | 2155 | 3232 | 0.351 | 0.165 | 19600 |
| 4NL6 | 2253 | 3379 | 0.351 | 0.165 | 20450 |
| 4NL7 | 3346 | 5019 | 0.351 | 0.165 | 30490 |
| 4NL8 | 2951 | 4427 | 0.351 | 0.165 | 26900 |
| 4NL9 | 3195 | 4793 | 0.351 | 0.165 | 29120 |
| 4NL10G | 2730 | 4094 | 0.351 | 0.164 | 24970 |
| Mean | 2727 | 4091 | | 0.165 | 24850 |
| St. Dev. | 413 | 620 | | 0.000 | 3763 |
| COV | 15.1% | 15.1% | | 0.3% | 15.1% |

As for the monolithic glass specimens without a hole, this specimen set establishes the base strength of the $1/2\ inch$ laminated glass specimens. It was determined that the mean strength of this specimen type is $\sigma_{ult-lam} = 24850\ psi$ with the coefficient of variation $COV = 15.1\%$. There is a wider range in breakage values because three specimens (4NL3M, 4NL5, 4NL6) broke differently than the other seven specimens. Each glass

laminate shattered independently during the breakage of those three specimens, whereas for the remaining specimens, both laminates shattered instantaneously. If the three values were removed from the statistics, the average strength of the glass specimens without a hole would be $\sigma_{ult-lam} = 27080\ psi$, and the coefficient of variation $COV = 6.9\%$.

**Table 20: Strength of Laminated Glass – 4pt. Bending – With Hole.**

| Laminated Glass - 4pt. Bending - with Hole | | | | | | |
|---|---|---|---|---|---|---|
| Specimen # | Load (lbf) | $M_{max}$ (lbf-in) | $t_{eff}$ (in) | $S_{net}$ ($in^3$) | $\sigma_{net}$ (psi) | $\sigma_{peak}$ (psi) |
| 4HL1 | 1732 | 2598 | 0.351 | 0.129 | 20150 | 30980 |
| 4HL2 | 1821 | 2732 | 0.351 | 0.130 | 21090 | 32410 |
| 4HL3 | 1501 | 2252 | 0.351 | 0.132 | 17070 | 26240 |
| 4HL4 | 1667 | 2500 | 0.351 | 0.131 | 19030 | 29250 |
| 4HL5 | 1574 | 2361 | 0.351 | 0.131 | 17960 | 27600 |
| 4HL6 | 1368 | 2052 | 0.351 | 0.131 | 15670 | 24080 |
| 4HL7 | 1856 | 2784 | 0.351 | 0.130 | 21480 | 33010 |
| 4HL8 | 1758 | 2637 | 0.351 | 0.132 | 19920 | 30620 |
| 4HL9G | 1818 | 2727 | 0.351 | 0.130 | 21000 | 32280 |
| 4HL10G | 1844 | 2766 | 0.351 | 0.129 | 21380 | 32870 |
| Mean | 1694 | 2541 | | 0.131 | 19470 | 29930 |
| St. Dev. | 156 | 234 | | 0.001 | 1898 | 2917 |
| COV | 9.2% | 9.2% | | 0.9% | 9.7% | 9.7% |

The average breaking stress for $1/2\ inch$ laminated samples with a hole subjected to four-point bending is $\sigma_{hole-lam} = 29930\ psi$. This breaking stress is greater than that of laminated samples without a hole. This result is counterintuitive because the drilling procedure introduces flaws that decrease the strength of glass. The phenomenon that is observed in the test data evinces the opposite trend.

**Table 21: Strength of Laminated Glass – 3pt. Bending – With Hole.**

| Laminated Glass - 3pt Bending - with Hole | | | | | | |
|---|---|---|---|---|---|---|
| Specimen # | Load (lbf) | $M_{max}$ (lbf-in) | $t_{eff}$ (in) | $S_{net}$ ($in^3$) | $\sigma_{net}$ (psi) | $\sigma_{peak}$ (psi) |
| 3HL1 | 729 | 2551 | 0.351 | 0.129 | 19720 | 30310 |
| 3HL2 | 785 | 2748 | 0.351 | 0.129 | 21250 | 32660 |
| 3HL3 | 779 | 2728 | 0.351 | 0.130 | 21050 | 32360 |
| 3HL4 | 792 | 2770 | 0.351 | 0.129 | 21430 | 32950 |
| 3HL5 | 832 | 2912 | 0.351 | 0.129 | 22540 | 34640 |
| 3HL6 | 860 | 3008 | 0.351 | 0.130 | 23140 | 35570 |
| 3HL7 | 726 | 2541 | 0.351 | 0.129 | 19640 | 30190 |
| 3HL8 | 758 | 2653 | 0.351 | 0.131 | 20260 | 31140 |
| 3HL9G | 812 | 2842 | 0.351 | 0.130 | 21920 | 33680 |
| 3HL10G | 758 | 2651 | 0.351 | 0.129 | 20500 | 31510 |
| Mean | 783 | 2740 | | 0.130 | 21150 | 32500 |
| St. Dev. | 41 | 143 | | 0.001 | 1100 | 1691 |
| COV | 5.2% | 5.2% | | 0.4% | 5.2% | 5.2% |

As with laminated glass specimens with a hole subjected to four-point bending, this set of laminated specimens loaded via the fitting exhibits a greater average breaking stress $\sigma_{fitting-lam} = 32500\ psi$ than the basic strength of plain laminated glass specimens $\sigma_{ult-lam} = 24850\ psi$. The breaking strength of laminated glass specimens with a fitting is even greater than the average strength of laminated glass specimens with a hole $\sigma_{hole-lam} = 29930\ psi$. This tendency is also counterintuitive because a fitting introduces an additional layer of uncertainty and concentrated stresses. The expected trend is that the strength of glass with a fitting is lower than the strength of glass with a hole. The explanation as to why the stress of laminated glass specimens with a fitting is lower than those with an open hole may be due to the significant curvature that developed when loaded. Consequently, the applied force was not transferred to the exact center of a specimen as it is during theoretical three-point bending. Instead, these specimens were

subjected to "four-point" bending. The fitting pushed on the glass specimens at the farthest points of its perimeter, away from the transverse centerline. If the width of the fitting is subtracted from the three-point bending moment arm (i.e., four-point bending moment formula is used), the reduced average breaking moment is $2278\ lbf - in$, and the average breaking stress is $27020\ psi$.

These unexpected results might be caused by the following elements: the effective thickness of laminated glass, the stress concentration factor, the problems with load reading, and the different mechanical properties of each set of glass specimens. First, calculating the effective thickness of laminated glass and stress concentration factors cannot influence the strength results because the strain gauge data were analyzed and compared to the predicted stresses. Because of the linear behavior of laminated glass, the common load of $1000\ lbf$ was used to compare stresses from the actual strain gauges, the stress concentration factor, and the Finite Element Model. The modulus of elasticity for glass $E = 10{,}400{,}000\ psi$ was used to convert the glass strain to stresses. This modulus of elasticity is also consistent with the modulus of elasticity obtained from the slope of load versus displacement graphs for monolithic glass specimens without a hole. Figure 44 shows stress versus distance from the edge of a hole for laminated specimens subjected to four-point bending. One can see that the stress predicted by Roark's formula coincides with Reissner's stress prediction, and both coincide with the strain gauge readings (within 8%). The finite element model stress prediction is consistent with Reissner's stress prediction as well. This indicates a very strong correlation between the stress concentration factor used for calculating the peak stresses and the stresses received

from the strain gauges. As a result, one can assume that the stress concentration factor predicts the correct breaking stresses.

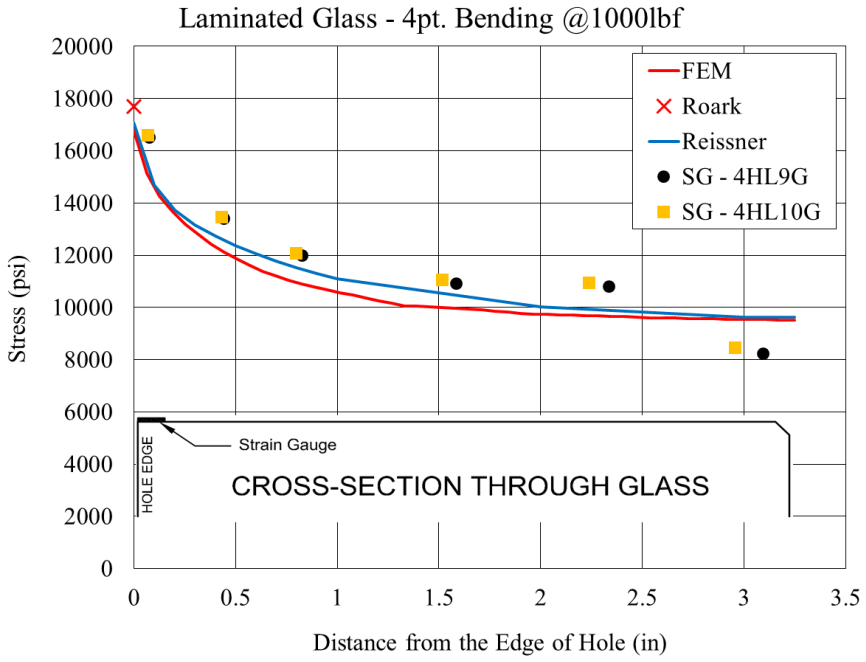


**Figure 44: Comparison of Stress Predictions for Laminated Glass.**

The remaining reasons for the unexpected stress results reside on the load reading inconsistencies and the different glass mechanical properties. Since the laminated glass specimens were tested along with the monolithic ones where no variation was observed, it is not likely that the laminated glass specimen readings were off. Therefore, the researcher surmised that the mechanical properties of the laminated glass varied for each specimen type influencing the overall strength of the glass specimens. This argument is also supported by the fact that each laminated glass specimen type arrived a month apart.

# 5. CONCLUSION

## 5.1. Summary

The first key finding of this Master's project is related to the evaluation of stress concentration around a hole in a glass specimen subjected to uniaxial bending. Reissner's thick plate theory on the stress concentration factor for an infinite plate, Roark's formula for the stress concentration factor for a finite width plate, the stress concentration factor from the Finite Element Model, and the actual stress concentration factor calculated from strain gauge data were compared. It was discovered that Reissner's stress concentration factor – Equation (7) – and Roark's stress formula for stress concentration factor – Equation (9) – are in accordance with the stress concentration factor from the FEM for plates wider than $5\ inches$. Their peak stress prediction differs from that of the FEM by $5.3 - 5.9$ % for narrow plates and by 1.6% for wide plates. The actual strain gauge stress concentration factor demonstrates that it is correct to assume that stress increases at the edge of hole. However, when matched with the previously mentioned stress concentration factors, the same values were not reached.

The second key finding concerns the maximum ultimate stress at which each specimen type broke. The basic strength of $1/2\ inch$ monolithic glass is $\sigma_{ult} = 29460\ psi$. The presence of a water-jet drilled hole reduces this strength by 3.3% to $\sigma_{hole-ult} = 28500\ psi$. If the glass is loaded via the fitting, which simulates real-life use of structural glass, the strength of the glass is reduced by an additional 12.5% to $\sigma_{fitting-ult} = 24820\ psi$. The very important takeaway from this finding is that chamfer at the edge of a hole cuts off the peak stress and introduces a new stress concentration factor for a

chamfered hole edge. The great advantage of chamfering the edge gives the designer an 18% increase in the moment capacity of a glass pane.

Unfortunately, the same findings did not occur for the laminated glass specimens. Laminated glass specimens exhibited misunderstood results. The average strength of $1/2\ inch$ plain laminated glass specimens is $\sigma_{ult-lam} = 24850\ psi$, whereas the average strength of laminated glass specimens with a hole is $\sigma_{hole-lam} = 29930\ psi$. The average strength of laminated glass specimens loaded via the fitting is $\sigma_{fitting-lam} = 32500\ psi$. This increase in strength is counterintuitive and not fully comprehensible. It is suspected that it is a result of the different mechanical properties of the PVB interlayer and the stress levels to which the second glass batch was tempered.

### 5.2. Conclusions

It was discovered that Roark's formula for the stress concentration factor – Equation (9) – predicts accurate peak stresses at the edge of hole of a glass plate subjected to out-of-plane bending. This Equation (9) can be used as a simple tool to assess the stresses around a hole instead of a complex Finite Element Analysis. The stresses predicted by Roark's formula are in accordance with the Finite Element Model stresses and the stresses obtained from strain gauge data.

Additionally, a new discovery was made regarding the level of strength of monolithic glass. The strength of monolithic glass decreases as it moves away from its simplest form. It is strongest as a plain sheet of glass; its strength then decreases with the presence of a hole. The glass continues to lose its strength when it is loaded via fitting. However, if the edge of a hole is chamfered, the peak stresses are altered and an additional 18%

increase in moment capacity is obtained. It is good practice for glass manufacturers to chamfer the hole edges to increase the capacity of four-point-supported glass panes.

Conversely, the strength of laminated glass is not fully understood and demands further research to truly understand and explain the varying and counterintuitive strength results.

To conclude, both the monolithic and laminated glass specimens broke at much higher stress levels than the ASTM E1300 specifies as the edge strength of fully tempered glass.

### 5.3. Open Questions

There are still many unknowns at the completion of this research project because the behavior of glass in many innovative applications is still not fully understood. As far as point-supported glass is concerned, the next step in research would be to investigate the behavior of an entire four-point-supported glass pane as a larger unit. In this research project, the specimens are only a snapshot of the corner area where diagonal bending occurs. Further research should also explore whether the strength results presented in this research correlate with the overall strength of the full scale glass panes.

The laminated glass results did not indicate a consistent pattern in behavior that would lead to a thorough understanding of its characteristics. The inconsistent results in strength raise even more questions regarding the behavior of this type of glass. Additional testing is required to shed more light on the elements that can affect the strength of laminated glass. It would be advisable to test more plain specimens without a hole to gain a solid understanding of the strength of laminated glass. It is also imperative to obtain tempering readings for each specimen in order to understand any anomalies in glass behavior.

Because of the limited amount of time and resources available for this project, a few minor changes could be made to improve future research. The fourth-order polynomial function utilized as a curve fit to predict the stress peak right at the edge of a hole seems to underestimate the actual increasing trend of the peak stress. A slight dip in value at the very edge of a hole is noticeable. With more advanced mathematical formulation, a more precise peak stress value could be obtained from the strain gauge data.

The author of this research project would also like to further explore the stress concentration factor for thick plates with large deflection. During the search for classical method approaches, no stress concentration factor for thick plates with large deflections was found. His interest resides in the difference between the obtained stress concentration factor from Reissner's work or Roark's formulas and this large deflection stress concentration factor.

## REFERENCES


[1] Hadkova, J. (Director). (7 May 2010). Deset Stoleti Architektury – Vila Tugendhat *[Documentary film]*. PR Agentura (Producer). Prague, The Czech Republic.

[2] Gaffer, Corey. 2013. "SR Crown Hall (B&W) – Mies Van Der Rohe." [Internet, WWW]. *Available:* Available from the Corey Gaffer Photography Stills • Motion website; *Address:* http://www.gafferphotography.com/prints/ko8tacthygx15eu85vxo526nlypmr1; [Accessed: 7 April 2016]. A copy of this photo is available from the author.

[3] "Louvre." 22 June 2016. Wikipedia: The Free Encyclopedia. [Internet, WWW]. *Available*: Available from the Wikipedia website; *Address:* https://en.wikipedia.org/wiki/Louvre; [Accessed 22 June 2016].

[4] "30 St. Mary Axe." 21June 2016. Wikipedia: The Free Encyclopedia. [Internet, WWW]. *Available*: Available from the Wikipedia website; *Address*: https://en.wikipedia.org/wiki/30_St_Mary_Axe; [Accessed 22 June 2016].

[5] "Roman Catholic Diocese of Orange." 17 January 2016. Wikipedia: The Free Encyclopedia. [Internet, WWW]. *Available*: Available from the Wikipedia website; *Address*: https://en.wikipedia.org/wiki/Roman_Catholic_Diocese_of_Orange; [Accessed 12 December 2015].

[6] Wallpaper Abyss. 2016. "14 The Louvre Wallpapers." [Internet, WWW]. *Available:* Available from the Wallpaper Abyss – Alpha Coders website; *Address*: https://wall.alphacoders.com/by_sub_category.php?id=212553; [Accessed 9 April 2016].

[7] Patterson, Michael R. May 2008. "Structural Glass Facades: A Unique Building Technology." Master's Thesis, University of Southern California.

[8] Joshua Schultz, Douglas Stahl, and Christian Stutzki. September 2012. "Experimental Investigation of Numerical Design Method for Point-Supported Glass." *Journal of Architectural Engineering* Vol 18, No. 3: pp. 223-232.

[9] Stutzki Engineering, Inc. Home Page. [Internet, WWW]. Address: https://www.stutzkiengineering.com.

[10] Stutzki Engineering, Inc. 3 March 2016. *Stutzki Engineering Database*. Milwaukee, WI: Stutzki Engineering, Inc. A copy of this database is in Stutzki Engineering's possession, but the database is not available for public viewing. For details, please contact the author at cervenkaj@msoe.edu.

[11] SADEV. 17 May 2016. *Swivel Fitting Sketch*. Keokuk, IA: SADEV. A copy of this document is in SADEV's possession, but the document is not available for public viewing. For details, please contact the author at cervenkaj@msoe.edu.

[12] Alisbo, Leoven. January 2015. "Glass Manufacture." *Inorganic Materials* Vol. 9, pp. 1-6.

[13] Kalogeras, Ioannis M. and Lobland, Haley E. Hagg. 2012. "The Nature of the Glassy State: Structure and Glass Transitions." *Journal of Materials Education* Vol. 34 (3-4), pp. 69-94.

[14] Office of Air Quality Planning And Standards, Office of Air And Radiation, and U.S. Environmental Protection Agency. January 1995. *Compilation of Air Pollutant Emission Factors.* Research Triangle Park, NC: U.S. Environmental Protection Agency.

[15] Maniatis, Iris. 2005. "Numerical and Experimental Investigations on the Stress Distribution of Bolted Glass Connections under In-Plane Loads." Ph.D. diss., Technische Universität München.

[16] British Standard Institution. February 2012. *Glass in Building. Basic Soda-Lime Silicate Glass Products. Definitions and General Physical and Mechanical Properties.* Designation: EN 572-1. In Annual Book of EN Standards 2012. Brussel: European Committee for Standardization.

[17] British Standard Institution. September 2004. *Glass in Building. Special Basic Products. Borosilicate Glasses. Definition and General Physical and Mechanical Properties.* Designation: EN 572-1. In Annual Book of EN Standards 204. Brussel: European Committee for Standardization.

[18] Nielsen, Jens H. 2009. “Tempered Glass – Bolted Connections and Related Problems.” Ph.D. diss., Technical University of Denmark.

[19] Glazette. 2016. "Annealed Glass." [Internet, WWW]. *Available:* Available from the Glazette website; *Address:* http://www.glazette.com/Glass-Knowledge-Bank-79/Annealed-Glass.html; [Accessed: 22 June 2016].

[20] Carlen Glass Merchants Ltd. 2015. “Toughened Glass.” [Internet, WWW]. *Available:* Available from the Carlen Glass Merchants Ltd. Fire Glass Specialists website; *Address:* http://www.carlenglass.ie/services/toughened-glass/#prettyPhoto/3/ [Accessed: 7 April 2016]. A copy of this photo is available from the author.

[21] ASTM International. 2012. *Standard Specification for Heat-Strengthened and Fully Tempered Flat Glass.* Designation: ASTM C1048. In Annual Book of ASTM Standards 2012. West Conshohocken, PA: ASTM International.

[22] Shin-ichi, Aratani [inventor]. 11 July 1989. “Chemically Strengthened Glass Article and Method of Producing Same.” United Kingdom Patent 4,846,868.

[23] Mecholsky, John. 14 October 2008. "Mechanical Properties of Glass." Lecture number 12 at the Lehigh University, Pennsylvania.

[24] American Architectural Manufacturers Association. February 2011. *Structural Properties of Glass.* Designation: AAMA CW-12-84. Schaumburg, IL: AAMA

[25] De Gaetano, Sergio, Matthias Hladimann, and Mauro Overend. February 2007. “Diagnostic Interpretation of Glass Failure.” *Structural Engineering International*, pp. 151-158.

[26] ASTM International. 2012. *Standard Practice for Determining Load Resistance of Glass in Buildings.* Designation: ASTM E1300. In Annual Book of ASTM Standards 2012. West Conshohocken, PA: ASTM International.

[27] Bernard, Fabrice, Laurent Daudeville, and Rene Gy. “Residual Stresses Near Holes in Tempered Glass Plates.”

[28] Institute for Interconnecting and Packing Electronic Circuit. 1998. *IPC-TM-650 Test Methods Manual.* Order Number: 2.4.24.5. Northbrook, IL: IPC

[29] Glass Association of North America. 2007. "How Laminated Glass Is Made with PVB." [Internet, WWW]. *Available:* Available from the GANA website; *Address:* http://www.glasswebsite.com/video/laminating.asp; [Accessed: 15 October 2015].

[30] ASTM International. 2014. *Standard Specification for Laminated Architectural Flat Glass.* Designation: ASTM C1172-14. In Annual Book of ASTM Standards 2012. West Conshohocken, PA: ASTM International.

[31] Knowles, John. Project Engineer, Stutzki Engineering. 18 January 2016. Conversation with the author, Milwaukee, WI.

[32] ASTM International. 2013. *Standard Practice for Design and Performance of Supported Laminated Glass Walkways.* Designation: ASTM E2751. In Annual Book of ASTM Standards 2013. West Conshohocken, PA: ASTM International.

[33] Matthias Haldiman, Andreas Luible, and Mauro Overend. *Structural Use of Glass.* ETH Zurich and Internation Association for Bridge and Structural Engineering, Zurich, 2008.

[34] Schneider, Jens, Johann D. Worner, June 2001. "Glass Strength of Annealed and Tempered Structural Glass in the Area of Drilled Holes." *Glass Processing Days*, pp. 193-198.

[35] Bength, Camilla. 2005. "Bolt Fixings in Toughened Glass." Master's thesis, Lund University, Lund, Sweden.

[36] Froling, Maria. 2011. "Strength Design Methods for Laminated Glass." Ph.D. diss., Lund University, Lund, Sweden.

[37] Timoshenko, S. and S. Woinowsky-Krieger. January 1959. *Theory of Plates and Shells*. McGraw-Hill: New York.

[38] Young, W. C. and R. G. Budynas. 2002. *Roark's Formulas for Stress and Strain*. McGraw-Hill: New York.

[39] Wang, Chien Ming. 2001. "Deducing Thick Plate Solutions from Classical Thin Plate Solutions." *Structural Engineering and Mechanics* Vol. 11, pp. 89-104.

[40] "Thin versus Thick Shells." 20 December 2015. [Internet, WWW]. *Available:* Available from the DocFoc website; *Address:* http://www.docfoc.com/thin-vs-thick-shells; [Accessed: 25 January 2016].

[41] Reissner, Eric. June 1945. "The Effect of Transverse Shear Deformation on the Bending of Elastic Plates. *ASME Applied Mechanics* Vol. 67, pp. 69 – 77.

[42] Pilkey, Walter D. and Deborah F. Pilkey. 2008. *Peterson's Stress Concentration Factors.* John Wiley & Sons: New Jersey.

[43] Abaqus. 2011. Dassault Systèmes, Providence, RI, USA

[44] ASTM International. 2012. *Standard Test Methods for Strength of Glass by Flexure (Determination of Modulus of Rupture).* Designation: ASTM C158-02. In Annual Book of ASTM Standards 2012. West Conshohocken, PA: ASTM International.

## APPENDIX A: Load Versus Displacement Plots

In this appendix, graphs of load versus displacement are presented. It is very clear that both monolithic and laminated glass behave linear-elastically. Each specimen type contains ten replicates. However, because of a technical error, the linear vertical displacement was incorrectly recorded for four replicates of monolithic glass specimens with no hole loaded using the four-point bending test setup. Only six plots are displayed in Figure A-1.

Three specimens of the laminated glass group with no hole subjected to four-point bending evinced a two-stage failure. Each glass ply broke separately creating a step in the otherwise perfectly linear graph. This phenomenon is showed in Figure A-2. The general observation that was made is that laminated glass of the same nominal thickness ($1/2\ inch$) is less stiff than monolithic glass of the same thickness. This behavior is expected because laminated glass does not behave as a perfectly solid material, but rather acts as a laminated cross-section.

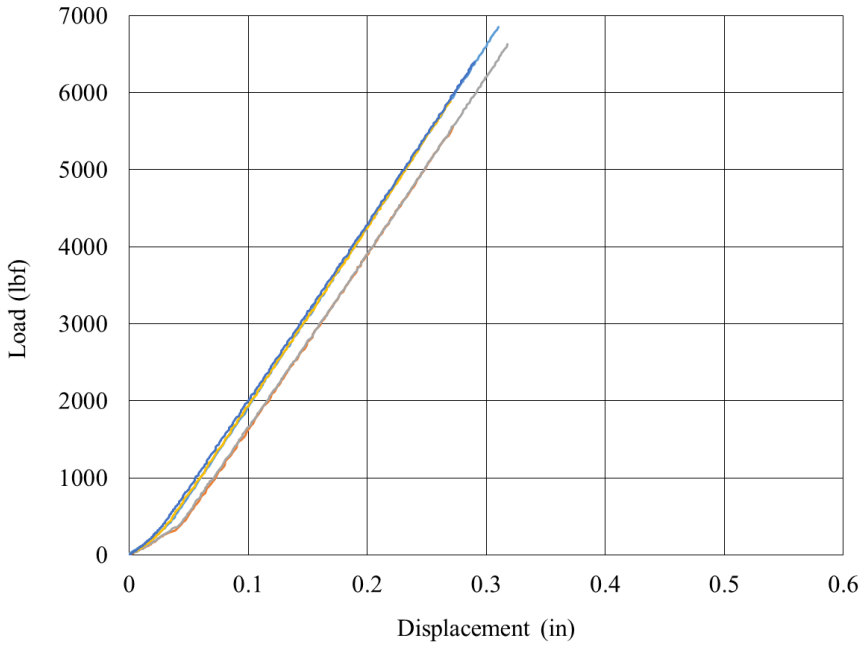


**Figure A-1: Monolithic Glass with No Hole – 4pt. Bending.**

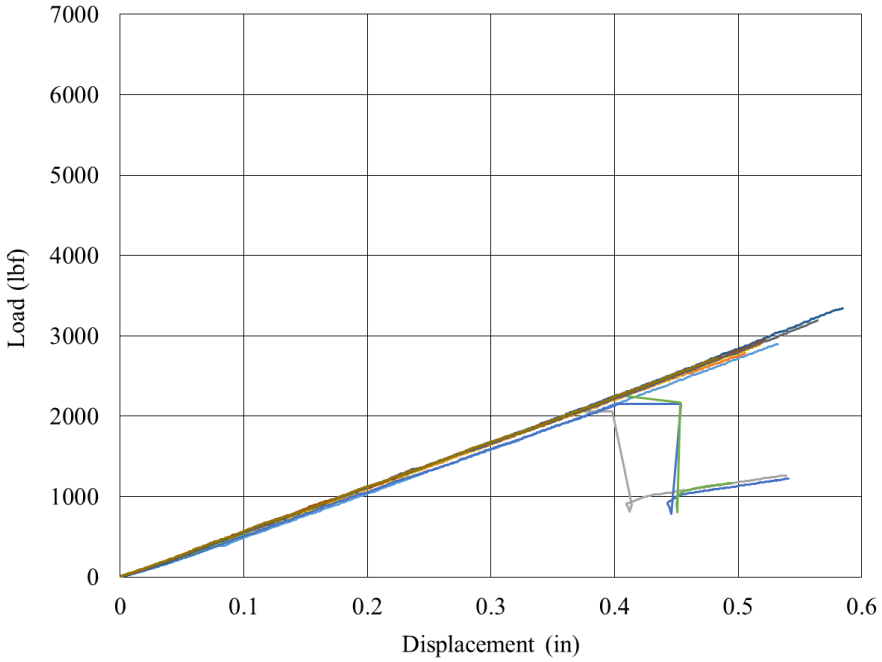


**Figure A-2: Laminated Glass with No Hole – 4pt. Bending.**

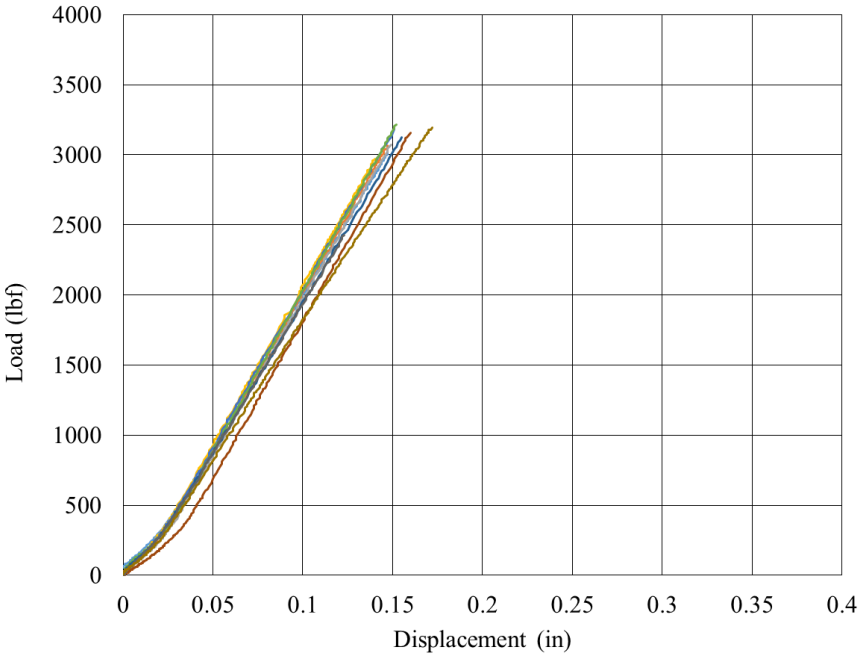


**Figure A-3: Monolithic Glass with Hole – 4pt. Bending.**

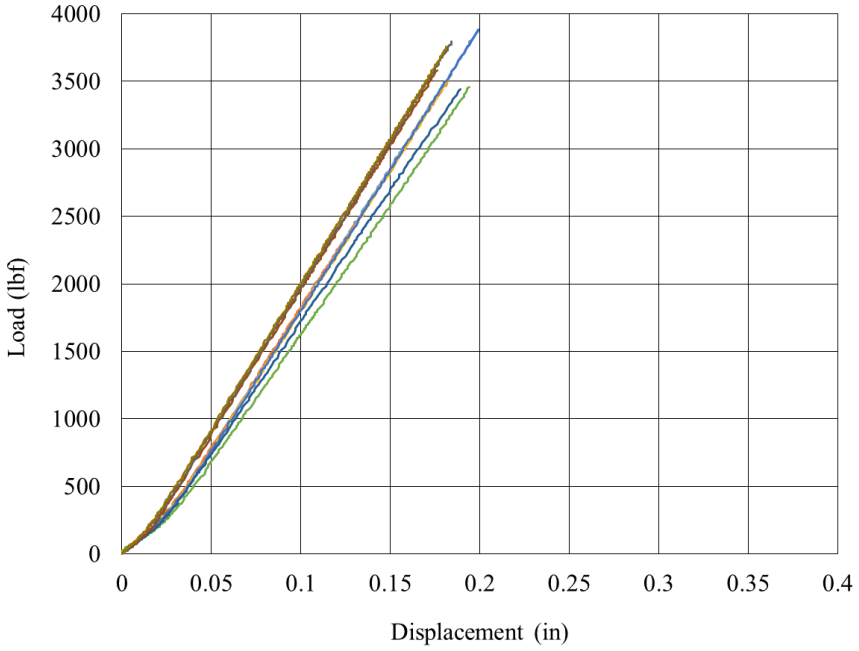


**Figure A-4: Monolithic Glass with Chamfered Edge of Hole – 4pt. Bending.**

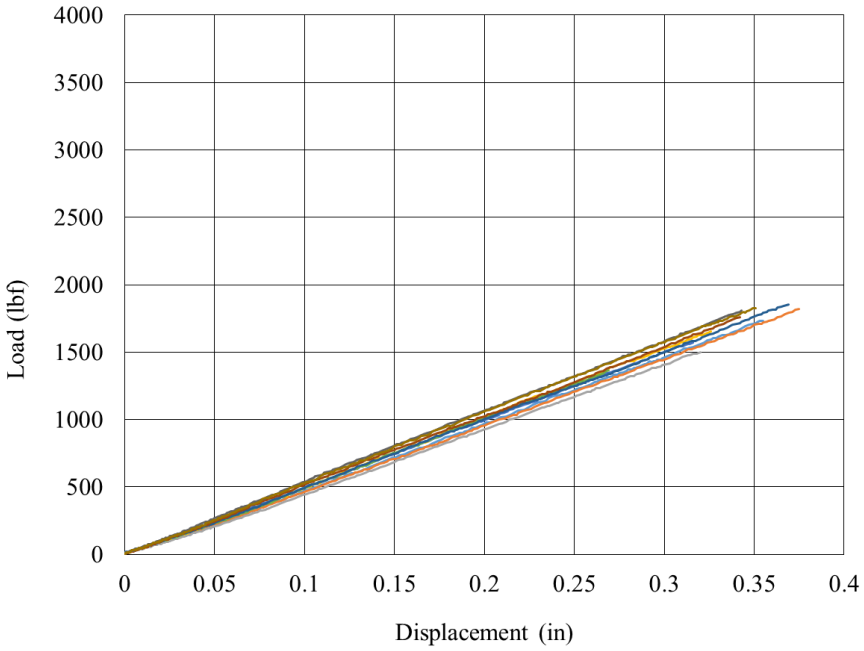


**Figure A-5: Laminated Glass with Hole – 4pt. Bending.**

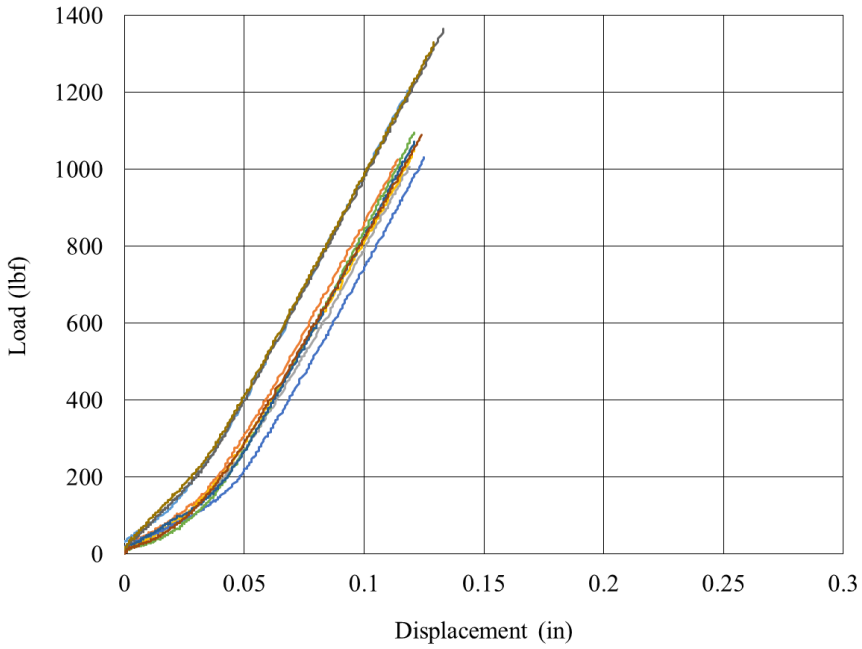


**Figure A-6: Monolithic Glass with Fitting – 3pt. Bending.**

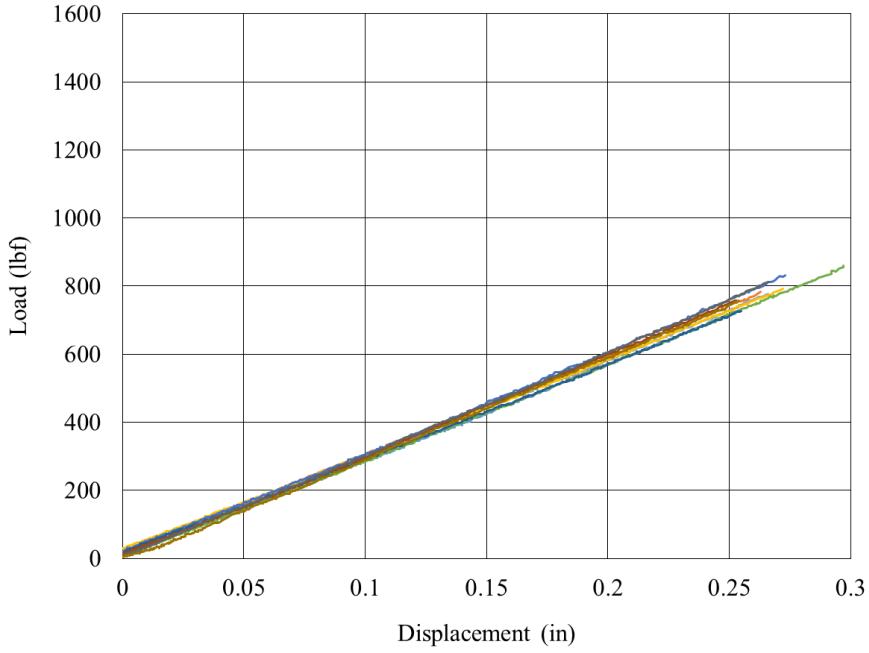


**Figure A-7: Laminated Glass with Fitting – 3pt. Bending.**